DOI: 10.26599/FSHW.2026.9251066

Contents lists available at SciOpen

Food Science and Human Wellness

journal homepage: https://www.sciopen.com/journal/2097-0765

China Food Publishing Co.

Protective effects of *Coreopsis tinctoria* flower extract on high-fat and high-fructose diet-induced cognitive deficit: Insight into gut microbiota-derived tryptophan metabolism

Le Sun[a,1], Jingxian Huang[a,1], Wenjie Wang[a, 1], Ming Chao[a], Yaya Chen[a], Pei Ma[a,*], Lijia Xu[a,b,*], Peigen Xiao[a,b]

[a] *Institute of Medicinal Plant Development, Chinese Academy of Medical Sciences and Peking Union Medical College, Beijing, 100193, China*

[b] *Hainan Branch of the Institute of Medicinal Plant Development, Chinese Academy of Medical Sciences and Peking Union Medical College, Haikou 570311, China*

ABSTRACT: The long-term high-fat and high-fructose diet (HFFD) exacerbates cognitive decline and gut microbiota disorder. *Coreopsis tinctoria* flower (CTF), grown at high altitudes, has been revered as a popular health-enhancing tea modulating glycolipid metabolism in Chinese. However, the neuroprotective effects of CTF against HFFD-induced cognitive decline remain to be elucidated. The present study investigated the hypothesis that the neuroprotective benefits of CTF are mediated by tryptophan metabolism derived from gut microbiota. The phytochemical characterization of CTF was performed by LC-MS/MS-assisted feature-based molecular networking method. Behavioral, neurophysiological and metabolic evaluations demonstrated CTF improved glycolipid metabolic disorders and cognitive decline in HFFD-fed mice. Integrative 16S rRNA sequencing and metabolomics analysis revealed CTF modulated the abundance of specific gut microbial genera (e.g., *Colidextribacter*) and enhanced gut bacteria-dependent tryptophan metabolites (especially indole-3-lactic acid and indole-3-carboxylic acid) levels in the hippocampus. Notably, antibiotic-induced depletion of microbiota abolished these metabolite changes and the neuroprotective effects of CTF, confirming the crucial role of the intestinal microbiota. Additionally, the protective effects of ICA and ILA on D-glucose induced synaptic damage in SH-SY5Y cells have been identified directly. These findings highlight the importance of microbiota-regulated tryptophan metabolism as a key mechanism behind the cognitive benefits of CTF, demonstrating its potential for managing metabolic disorder–related neurodegenerative conditions.

Keywords: *Coreopsis tinctoria* Nutt; High-fat and high-fructose diet; Cognitive deficit; Gut microbiota; Tryptophan metabolism

1. Introduction

The Western -style calorie-rich diet is featured with an abundant levels of fructose, cholesterol, and saturated fatty acids, which is frequently linked to metabolic syndromes (Christ et al., 2019). More alarmingly, a long-term high-fat and high-fructose diet (HFFD) is relevant with a 40% increased risk of cognitive decline (Dalile et al., 2022). Mild to moderate cognitive impairment, without early prevention and intervention,

[1] Co-first authors. These authors made an equal contribution to this work.
*** Corresponding author**
xulijia@hotmail.com (Lijia Xu); pma@implad.ac.cn (Pei Ma)

Received 10 July 2025
Received in revised from 20 August 2025
Accepted 8 December 2025

possibly develops into Alzheimer's disease (AD) or dementia (Zhang et al., 2017). However, no effective cure currently exists for cognitive decline. Therefore, developing more effective and safer preventive treatments for HFFD-caused cognitive deficit is possibly a critical strategy to delay and avoid the deterioration of the condition.

Recently, the gut-brain axis has been recognized as a vital pathway in regulating cognitive function (Agustí et al., 2018). Gut microbiota profoundly influences host brain physiology through multiple mechanisms, including immune modulation, endocrine signaling, and production of microbial metabolites (Liu et al., 2020). Among these, tryptophan (Try) metabolism by gut microbes plays a pivotal role in generating neuroactive compounds (Xue et al., 2023). These substances are capable of passing through the blood-brain barrier (BBB), activating aromatic hydrocarbon receptors (AHR) signaling to initiate neuroprotective outcomes (Sun et al., 2022). For instance, psychobiotic-derived indole-3-lactic acid (ILA) regulated AHR signaling activation to alleviate neuroinflammation and depression (Qian et al., 2024). Indole-3-propionic acid (IPA) effectively suppresses hippocampal microglial overactivation, thereby preventing excessive synaptic pruning in neurons via modulation of the AHR/NF-κB signaling pathway (Wang et al., 2023). Likewise, indoles comprising indole-3-acetic acid (IAA), indole-3-propionic acid (IPA) and indole, upregulated the AHR production and inhibited neuroinflammation (Sun et al., 2022). Hence, the gut microbiota and its TRYs, especially related indole derivatives, may represent promising reservoirs for the development of new interventions against HFFD-associated cognitive decline.

Coreopsis tinctoria Nutt. flower (CTF), commonly known as Snow Chrysanthemum, belongs to the *Asteraceae* family and is a widely consumed herbal tea. (Liu et al., 2023). CTF originated in North America, was introduced into China around 1900, and is mainly grown at altitudes exceeding 3000 meters in the Karakorum Mountains, Xinjiang, China, particularly in the Hotan area (Shen et al., 2021). CTF has been traditionally used by Indigenous peoples of India to treat diarrhea, pain, and bleeding, and in Portugal to manage diabetes (Liu et al., 2023). In China, it is known for its lipid- and glucose-regulating properties (Shen et al., 2021). CTF has multiple phytochemical components, mainly including flavonoids, phenolic acids, and terpenoids (Guo et al., 2022). Modern pharmacology suggests that CTF extracts and its bioactive compounds demonstrate neuroprotective properties *in vitro* and *in vivo* (Shen et al., 2021). CTF extracts can attenuate LPS-induced microglial activation by reducing pro-inflammatory cytokines and NF-κB signaling, and improve cognitive decline and oxidative stress in D-galactose-induced aging models (He et al., 2020). Recent studies also suggest that CTF polyphenols exert prebiotic-like effects, restoring gut microbiota composition and improving metabolic disorders such as type 2 diabetes (Liu et al., 2023). Despite these encouraging findings, whether CTF exerts cognitive protective effects in HFFD-induced models and how these effects are related to gut microbiota remain largely unexplored.

Therefore, this study aimed to investigate whether CTF supplementation can alleviate HFFD-induced cognitive impairment and whether its effects depend on the gut microbiota and microbial-derived tryptophan metabolites (TRYs). We conducted a comprehensive phytochemical analysis of CTF using LC-MS/MS

combined with feature-based molecular networking (FBMN), and evaluated its effects on behavior, metabolism, and neurophysiology in HFFD-fed mice. Multi-omics approaches, including 16S rRNA gene sequencing and targeted metabolomics, were employed to explore the role of gut microbes and their TRYs. Antibiotic intervention was further used to verify the involvement of the microbiota. Our findings provide new insights into the gut-brain axis mechanism by which CTF improves metabolic-associated cognitive decline, highlighting the potential of microbiota-targeted interventions for neurodegenerative disease prevention.

2. Materials and Methods

2.1 Materials and chemical reagents

The CTF plant was purchased from a marketplace in Dabancheng (Xinjiang Uyghur Autonomous Region, China). All fresh CTF materials were powdered and sieved through a 50-mesh sieve. Fifty-nine authentic standards of CTF were purchased from ChemFaces (Wuhan, Hubei, China) or Yongjian Pharmaceutical Co., Ltd. (Jiangsu, China). The specifics of the phytochemicals obtained are shown in Table S1. The Try and TRYs standards were provided from Macklin Biochemical Co., Ltd. (Shanghai, China). Chromatographic-grade solvents, such as acetonitrile, methanol and formic acid (FA) were supplied by Fisher Scientific (Fair Lawn, NJ, USA). Metformin (Met, purity ≥ 99%) was derived from MerckSerono (Shanghai, China).

2.2. Preparation and chemical characterization of CTF sample

The powder of CTF materials (10.0 kg) was soaked with 10 L of 80% ethanol at room temperature overnight and extracted three times. The supernatant evaporated to dryness. The samples were frozen and lyophilized. The lyophilized dry powder of CTF (0.1 g) was dissolved in 50% ethanol (8.5 ml) for LC-MS/MS procedure. The details of the qualitative and quantitative analysis, as well as methodology validation, are described in the supporting information.

2.3. Animal treatment and experimental process

All 72 male C57BL/6J mice (24 ± 2 g, 9 weeks old) were offered by the Sipeifu Biotechnology Co., Ltd. (Beijing, China) [Approval ID: SLXD-20231019015]. Prior to the experiment, all mice were acclimatized for 1 week, with free access to food and water (24°C ± 1°C; 55 ± 5% humidity, 12 h light/dark cycle). Then, the mice were randomly assigned to synchronize gut microbiota and reduce inter-individual heterogeneity (n = 12), which divided into the normal control group (NC), model group (HFFD), positive control group (Met, 200 mg/kg/day), as well as low dose (CTFL, 100 mg/kg/day), medium dose (CTFM, 200 mg/kg/day), and high dose (CTFH, 400 mg/kg/day) of CTF. Of note, the dosage administered to mice was determined by reference (Li et al., 2021; Li et al., 2014; Lv et al., 2023).

Except for the NC group given regular chow, the other five groups were all fed HFFD (10% fructose in drinking water) for 14 weeks to model cognitive deficit. The HFD with 60% fat was purchased from the Sipeifu Biotechnology Co., Ltd. All animal procedures complied with Chinese animal welfare ethics guidelines and were approved by the Animal Care and Experiment Committee of the Institute of Medicinal

Plant Development, Chinese Academy of Medical Sciences. Weekly recordings included mouse body weight, fasting blood glucose, and food/water intake. The oral glucose tolerance test (OGTT) and insulin tolerance test (ITT) were conducted in the final two weeks (supporting information).

2.4. Antibiotic (ABX) cocktail administration

The ABX cocktail experiment protocols mirrored earlier ones with minor modifications (Zhang et al., 2025). Nine weeks old male C57BL/6J mice (24 ± 2g) were randomly allocated into four groups (n = 12): HFFD, CTFH, AB, and AC. The dietary regimens for the HFFD and CTFH groups matched in section 2.3. The AB and AC groups mice were treated with ABX (Macklin Biochemical Co., Ltd.) containing streptomycin sulfate (0.5 mg/mL), neomycin sulfate (1 mg/mL), ampicillin (1 mg/mL), and gentamicin (1 mg/mL) to establish the pseudo-germ-free model. For the AC group, the ABX was administered in drinking water for seven days prior to receiving CTF (400 mg/kg) and continued during the remaining time to ensure the gut microbiota depletion.

2.5. Behavioral tests

A series of behavioral tests were conducted during the last two weeks of the experimental procedure. Behavioral assessments containing the open field test (OFT), Morris water maze (MWM) and Y-maze test were performed using previous methods (Pan et al., 2023; Zhang et al., 2025). All experimental animal behavior videos and parameter analyses were recorded by VisuTrack software (Shanghai Xinruan Information Technology Co., Ltd., Shanghai, China). The detailed procedure of behavioral experiments is presented in supporting information.

2.6. Sacrifice and Sampling of Mice

Upon completion of behavioral tests, the mice were anesthetized with tribromoethanol (i.v. 20 mL/kg via intraperitoneal injection) and euthanized. The whole brains were dissected and placed in 4% paraformaldehyde (n=5). The serum, hippocampal tissues, and cecal contents were gathered and placed at -80°C immediately for subsequent determination.

2.7. Hematoxylin & Eosin staining for histopathological assessment

A previous method in literature was referred (Zhang et al., 2025). The brain tissues were fixed in 4% paraformaldehyde, followed by ethanol dehydration, paraffin embedding, slicing, and hematoxylin and eosin (H&E) staining.

2.8. Transmission electron microscopy (TEM)

The TEM procedure followed published methods (Pan et al., 2023; Zhang et al., 2025) with modifications.. Hippocampus was fixed in 2.5% glutaraldehyde, washed with 0.1 M PBS and dehydrated in graded alcohol. Embedded and sectioned samples were dyed with 2% uranyl acetate in alcohol and observed under an HT-7800 TEM (30000×, HITACHI, Japan). Images were analyzed by Image J software (version 6.0, Media Cybernetics Inc., MD).

2.9. Untargeted metabolomics analysis of serum samples

The 100 μL aliquots serum were placed in 400 μL of cold protein precipitant (methanol/acetonitrile = 1:1, v/v) containing an internal standard (IS) to remove the protein. The supernatant was nitrogen-dried and redissolved in 100 μL protein precipitant. Sample (5 μL) were analyzed using UPLC-Q Exactive-Orbitrap HRMS with a C_{18} column (1.8 μm, 2.1 × 50 mm, Waters ACQUITY UPLC HSS T3, USA). The 0.1% FA in water and 0.1% FA in acetonitrile were mobile phase A and phase B, respectively. The gradient procedure was displayed in Table S2.

2.10. 16S rRNA sequencing

The microbial community analysis of mice feces through 16S rRNA was carried out by MetWare Biotechnology (Wuhan, China). Fecal genomic DNA from was extracted using the Vazyme DNA/RNA Extraction Kit (RM201-02), amplified by PCR targeting V3-V4 regions with the primer sequence of 515F (5'-GTGCCAGCMGCCGCGGTAA-3') and 806R (5'-GGACTACHVGGGTWTCTAAT-3'), and sequenced on the Illumina NovaSeq 6000 sequencer platform from Illumina (San Diego, CA, USA).

2.11. Widely targeted metabolomics analysis of stool samples

Widely targeted metabolomics of cecal content samples were analyzed by MetWare Biotechnology. In brief, 20 mg of cecal contents were transferred into 0.4 mL of 70% methanol solution containing an IS. The supernatant was analyzed by a UPLC-Triple Quad 5500 mass spectrometer installed with a Waters ACQUIY UPLC T3 column. Both water (solvent A) and acetonitrile (solvent B) were acidified with 0.1 % FA (v/v) for being employed as mobile phases at 0.4 ml/min. The optimized gradient elution program was depicted as Table S3.

2.12. Targeted tryptophan metabolomics

The Try pathway in targeted metabolomics of serum, feces and hippocampus samples was analyzed as in previous investigations (Desmons et al., 2022; Lefèvre et al., 2019; Wang et al., 2019). Briefly, the individual TRYs were prepared in a compound-free matrix to obtain a series of calibrators (0.10-50000.00 ng/ml). The 100 μL of serum or 5 mg of feces/hippocampus samples were taken, respectively, and homogenized with 400 μL of 80% methanol (contained IS). The supernatant was analyzed via the UPLC-Triple Quad 5500 mass spectrometer system after centrifugation. Phase A was 0.1% FA water with 5 mM ammonium acetate and phase B was 0.1% FA acetonitrile solution (Table S4 displayed the gradient elution procedure). The Waters ACQUIY UPLC C_{18} HSS T3 column was employed to separate TRYs. Inserting one QC sample every 6 sample intervals was performed for instrument stability testing. This method calculates the RSD of all QC samples based on the concentration of the standard to evaluate stability. The RSD ≤ 8% of the test result indicates that this method is stable and reliable (Table S8-S9). Target metabolite concentrations were quantified using calibration curves (Table S8). And the methodological validation was conducted according to previous methods (Desmons et al., 2022). The results of methodological validation were decrised in Table S9.

2.13. Real-time quantitative polymerase chain reaction (qRT-PCR) analysis and western blot (WB)

Hippocampal RNA was extracted by TriQuick Reagent, and the RNA integrity was assessed. Commercialized primers, including *Actb* (DMM404349), *Psd95* (DMM787665), *Snap25* (DMM289037), *Syp* (DMM820352), *Bdnf* (DMM358751), and *Ahr* (DMM795008) were purchased from XYbiotech (Shanghai, China).

The proteins from hippocampus and SH-SY5Y neuroblastoma cells were extracted using RIPA buffer with protease inhibitors, followed by WB analysis with the antibodies (Abcam, China): PSD95 (Postsynaptic density protein-95), SYP (Synaptophysin), SNAP25 (Synaptosome associated protein-25), BDNF (Brain-derived neurotrophic factor), GAPDH (glyceraldehyde-3-phosphate dehydrogenase), *β*-tubulin and *β*-actin. Membranes were visualized via the ChemiDoc Touch imaging system (Bio-Rad). Protein grayscale was analyzed using Image J (Zhang et al., 2025).

2.14. Immunofluorescent staining

Paraffin sections were blocked with 0.5% BSA, then incubated with primary antibodies against PSD95 (1:100) and AHR (1:100 dilution; ABclonal, China), followed by Alexa Fluor 488/594-conjugated anti-rabbit IgG (1:200, ab150077 and ab150080, Abcam). Nuclei were stained with DAPI (Servicebio, Wuhan, China) and sections were imaged under an Eclipse C1 upright fluorescence microscope (Nikon, Japan) with Caseviewer 2.4 software (3DHISTECH Ltd., Hungary).

2.15. SH-SY5Y cells culture and administration

The human neuroblastoma cell line SH-SY5Y was cultured in Dulbecco's modified Eagle's medium (DMEM) (Sigma-Aldrich, St. Louis, MO, USA) containing 4500 mg/L glucose, sodium pyruvate, and sodium bicarbonate; 10% fetal bovine serum, and penicillin and streptomycin at 100 U/mL penicillin and 100 mg/mL streptomycin (Sigma-Aldrich, St. Louis, MO, USA), and kept at 37°C in a humidified 5% CO_2 incubator. SH-SY5Y cells were obtained from ATCC, and all experiments were carried out up to 12 passages. In total, 80,000 cells/well were seeded on 96-well tissue culture plates. After 24 h, cells were treated with different concentrations of D-Glucose (Sigma-Aldrich, St. Louis, MO, USA) (25, 50, 75, 100, 150, and 200 mM) for 24 h to find out the maximum concentration that induce cytotoxicity. Cell viability was evaluated by incubating 100 μL of cell counting kit-8 (CCK-8) assay (0.1 mg/ml) for 2 h. The D-glucose concentration that substantially reduced cell viability was established as the optimal concentration. Groups were then established as follows: the control group comprised SH-SY5Y cells cultured with DMEM for 48 h; the model group comprised cells cultured with DMEM for 24 h prior to injury with 75 mM glucose for 24 h; the ILA and ICA group comprised cells simultaneously treated with ILA or ICA solution (Shanghai yuanye Bio-Technology Co., Ltd, Shanghai, China) (0-40 μM) and 75 mM D-glucose for 48 h.

2.16. Statistical assessment

Statistical analysis was conducted using GraphPad Prism 9.0 (San Diego, California, USA). Two-group comparisons used two-tailed unpaired Student's t-tests, while one-way/two-way ANOVA with Dunnett's post hoc tests evaluated multi-group differences. Non-normally distributed data were analyzed by Kruskal-Wallis

tests. Data are presented as the mean ± standard deviation (SD). All experiments were repeated ≥3 times, and $P < 0.05$ was considered significant.

3. Results

3.1. FBMN-assisted quali-quantitative profiling of CTF extract.

In the current study, the FBMN of phytochemical components in CTF was generated using the Global Natural Products Social Molecular Networking (GNPS) platform (Fig. 1). The representative total ion chromatograms (TIC) of CTF and the standard mixture were compared in the positive and negative ionization modes (Fig. 1A). Then, all 178 chemicals were putatively identified (mass errors < 5 ppm), 57 of which were first detected in CTF (Table S5), and 85 chemical nodes were annotated and dereplicated via the GNPS library (Fig. 1B-E and Table S5). Polyphenols, containing 78 flavonoids, 27 phenolic acids, 12 coumarins, and 10 other phenols, were the most numerous components discovered in CTF, accounting for 71.35% (Fig. 1F and Table S5), suggesting their importance as bioactive substances (Shen et al., 2021).

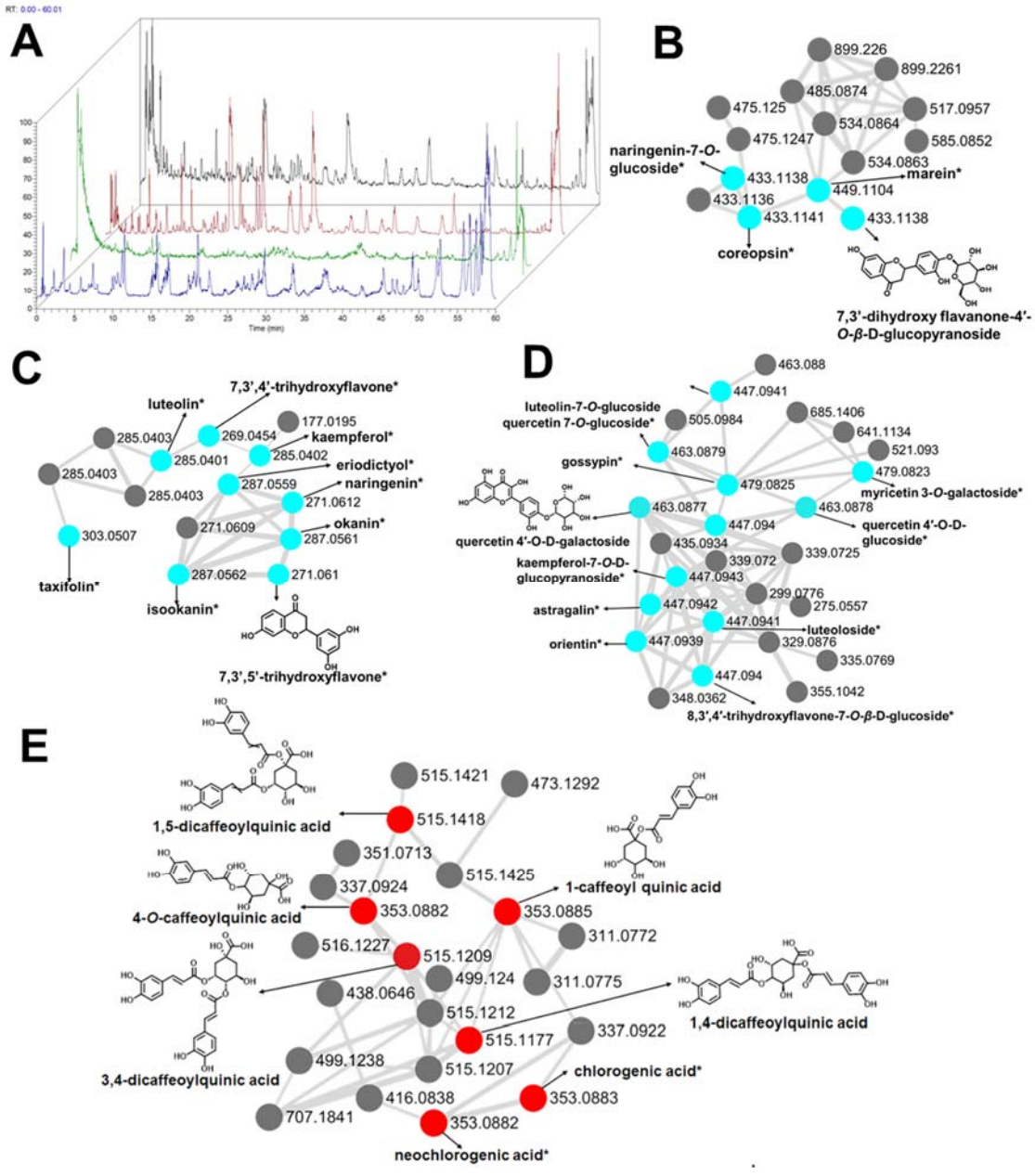

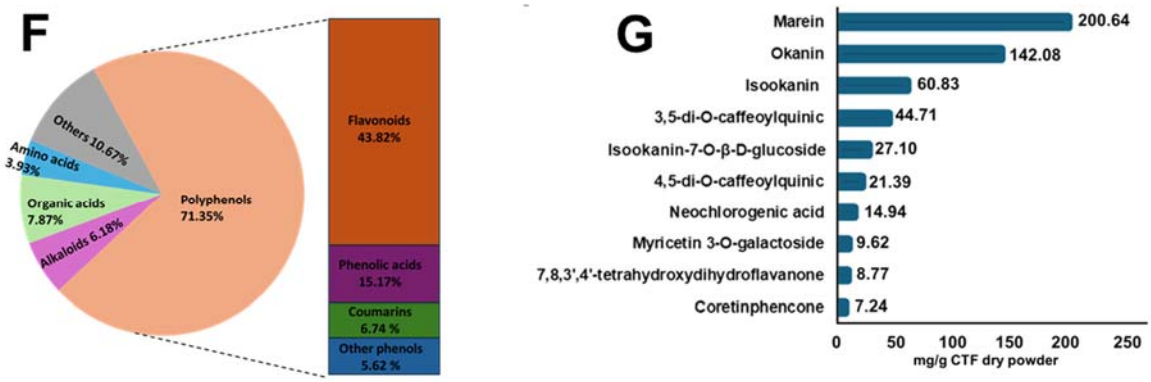

Fig. 1. The chemical profiles of *Coreopsis tinctoria* flower (CTF). (A) Total ion chromatogram of CTF extract and 59 standard mixtures (25.00 μg/mL) detected by the UPLC-Q-Exactive-Orbitrap HRMS system. The graph demonstrates CTF extract in the positive mode (black), standard mixture in the positive mode (red), CTF extract in the negative mode (green), and the standard mixture (blue) in the negative mode from top to bottom; (B-D) The representative FBMN of flavonoids in CTF; (E) The representative FBMN of phenolic acids in CTF. The edge width was defined by the cosine score (ranging from 0.7 to 1.0) between paired connected nodes. Compounds marked with asterisks represent standard substances, and their structural formulas are listed in Table S1. Additional details can be found on the GNPS website (for positive ion mode: https://gnps.ucsd.edu/ProteoSAFe/result.jsp?task=f15f2e20b51947cf9d01c836efd0da11 and for negative ion mode: https://gnps.ucsd.edu/ProteoSAFe/result.jsp?task=f49db1179e0e4c928fd746bf6ed593a4); (F) Proportion of different types of compounds identified in CTF; (G) The content of the top ten compounds in CTF. Abbreviations: CTF, *Coreopsis tinctoria* flower; UPLC-Q-Exactive-Orbitrap HRMS, Ultra High Performance Liquid Chromatography Quadrupole Exactive Orbitrap Mass Spectrometry; FBMN, feature-based molecular networking; GNPS, Global Natural Products Social Molecular Networking

Therefore, the contents of 59 phenolic constituents in CTF were absolutely quantified through UPLC-QQQ-Trap MS (Table S6). The quantitative method was examined through methodological analysis (Table S6-S7). As shown in Fig. 1G, the top ten abundant phenolic compounds in CTF were marein (200.64±2.10 mg/g), okanin (142.08±1.50 mg/g), isookanin (60.83±1.25 mg/g), 3,5-dicaffeoylquinic acid (44.71±1.02 mg/g), isookanin-7-*O*-*β*-D-glucopyranoside (27.10±0.54 mg/g), 4,5-dicaffeoylquinic acid (21.39±0.39 mg/g), neochlorogenic acid (14.94±0.18 mg/g), myricetin-3-*O*-galactoside (9.62±0.21 mg/g), 7,8,3',4'-tetrahydroxydihydroflavanone (8.77±0.13 mg/g), and coretinphencone (7.24±0.20 mg/g). Overall, CTF extracts are abundant in bioactive ingredients, providing a solid foundation for developing medicine and health-modifying food products.

3.2. CTF improved glucolipid metabolism disorder and cognitive dysfunction in HFFD-fed mice.

To assess the protective effects of CTF supplements against cognitive impairment, a chronic model was established by 14 weeks HFFD feeding (Fig. 2A). The three doses of CTF and Met alleviated excessive weight gain at different degrees compared with the HFFD group (Fig. S1A, $P < 0.05$). Notably, CTF didn't affect daily food and water intake (Fig. S1 B-C), indicating that the observed anti-obesity effects were not due to reduced caloric intake. In addition, the effects of CTF on alleviating lipid accumulation and serum lipids were partially observed (Fig. S1 D-E). Both OGTT and ITT tests further demonstrated that CTF enhanced glucose tolerance and insulin sensitivity (Fig. S1 F-I, $P < 0.05$). Correspondingly, a significant reduction in insulin resistance, as indicated by HOMA-IR, was observed in CTF-administrated mice (Fig. S1 J-L, $P < 0.01$). Together, these findings suggest that long-term CTF supplementation effectively ameliorates HFFD-induced disturbances in glucolipid metabolism.

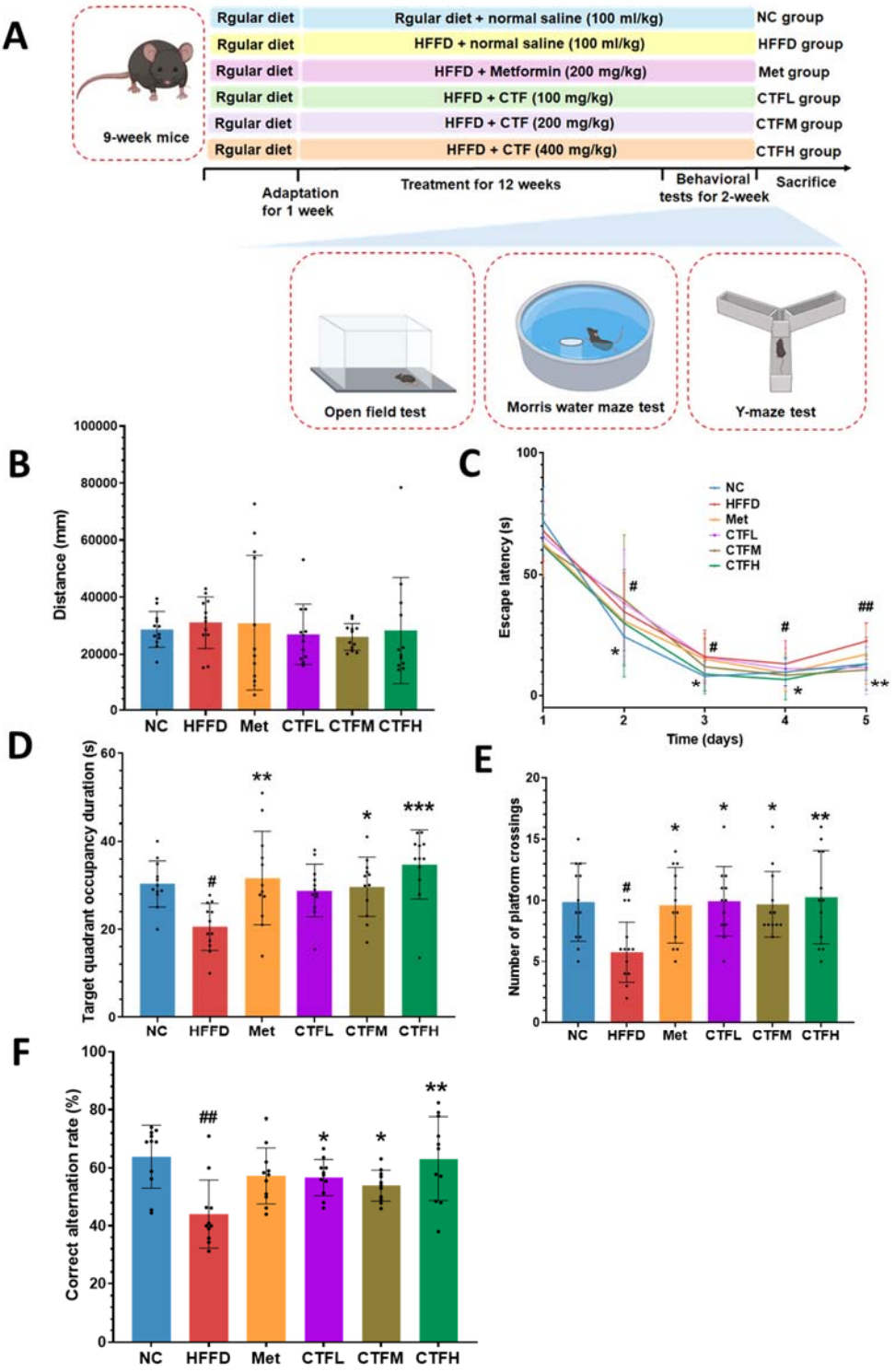

Fig. 2. CTF improved cognitive dysfunction in HFFD-fed mice (n=12). (A) Animal experimental design (n = 12); (B) Distance for 5 min in OFT; (C) Escape latency in MWM test; (D) Time spent in target quadrant in MWM test; (E) Number of platforms crossing in MWM test; (F) Spontaneous alternation rate in Y-maze test. Data are presented as the mean ± SD. #P < 0.05, ##P < 0.01, ###P < 0.001 in comparison to the control (NC) group, *P < 0.05, **P < 0.01, ***P < 0.01 in comparison to the HFFD group. p values were calculated by one-way ANOVA with Tukey's or Tamhane's tests. Abbreviations: HFFD, high-fat and high-fructose diet; OFT, the open field test; MWM, Morris water maze test.

To evaluate the hippocampus-dependent spatial learning and memory ability of HFFD-fed mice and the potential protective effects of CTF, the OFT, MMW, and Y-maze tests were conducted (Fig. 2A). There was no significant intergroup difference in total distance traveled during the OFT, indicating the motor ability of mice was not affected (Fig. 2B). During the 5-day place navigation test, escape latency trended downward,

though HFFD-group mice showed significantly higher latency than other groups from second day (Fig. 2C, $P < 0.05$). HFFD-group mice spent less time in the target quadrant during the probe trial (Fig. 2D, $P < 0.05$) and exhibited fewer platform crossings (Fig. 2E, $P < 0.05$), respectively less 42.85% and 40.82% than those in the NC group, indicating impaired spatial memory. These deficits were ameliorated by CTF, particularly at the high dose (400 mg/kg/day, $P < 0.001$ and $P < 0.01$). Fig. S1M showed the trajectories of each group in the space exploration test. Importantly, there were no significant differences in swimming speed among groups, ruling out motor dysfunction as a confounding factor (Fig. S1N). In the Y-maze test, mice in CTFH group showed 1.36 folds higher spontaneous alteration rate compared with the HFFD-fed mice (Fig. 2F, $P < 0.01$). These results indicated that CTF effectively alleviated HFFD-fed cognitive impairment, especially the CTF at the highest dose.

3.3. CTF ameliorated synaptic plasticity and neurotrophic factors in the hippocampus.

The structural plasticity of hippocampal postsynaptic membranes is fundamental to learning and memory (Zhang et al., 2025), and hippocampal neurons are particularly vulnerable to damage during cognitive decline. H&E staining revealed that neurons in the hippocampal dentate gyrus (DG) of HFFD-fed mice exhibited deep nuclear staining, reduced cell size, irregular morphology, and indistinct nuclear-cytoplasmic boundaries compared with the NC group; however, CTF markedly improved damaged neuronal morphology (Fig. 3A).

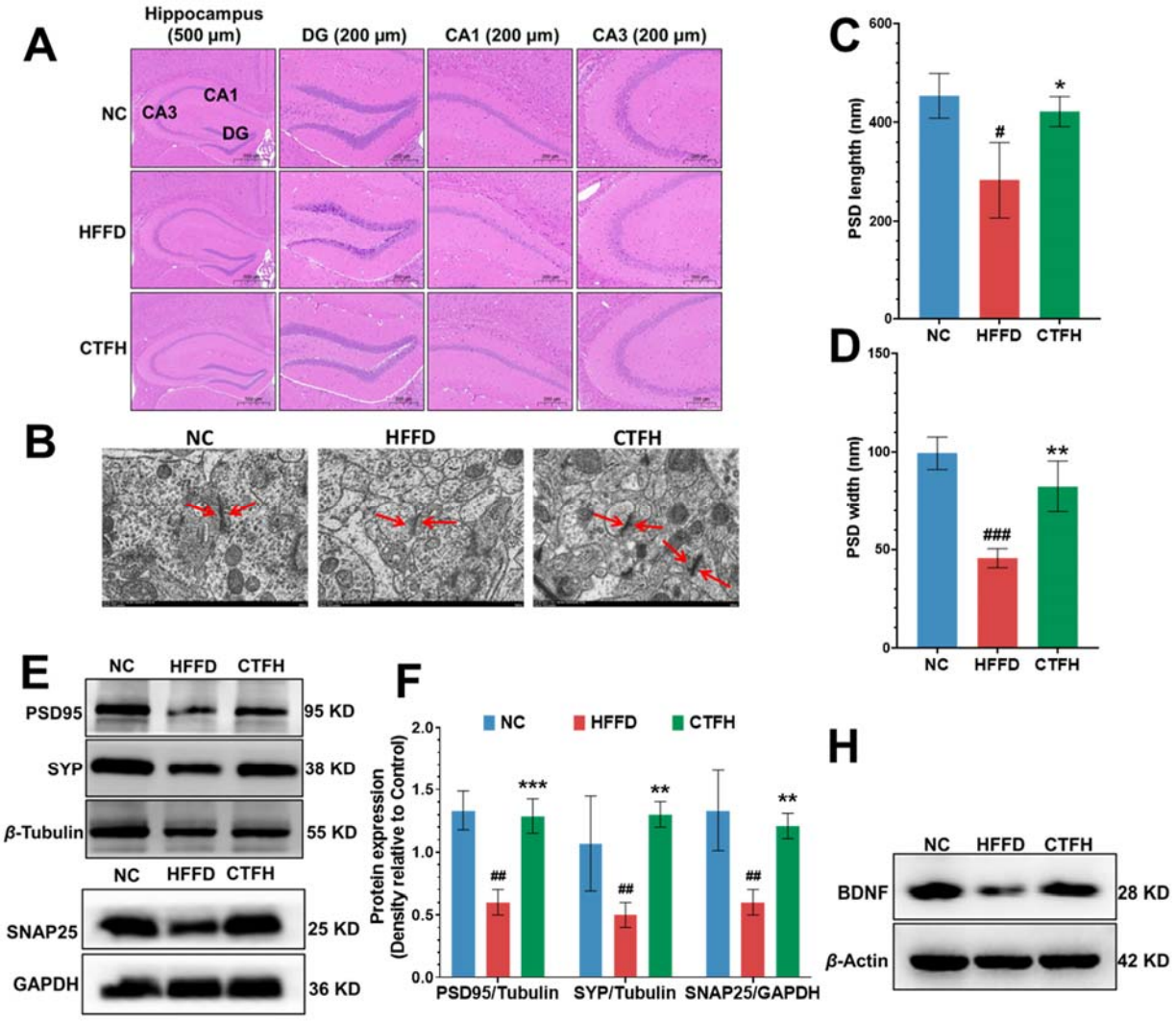

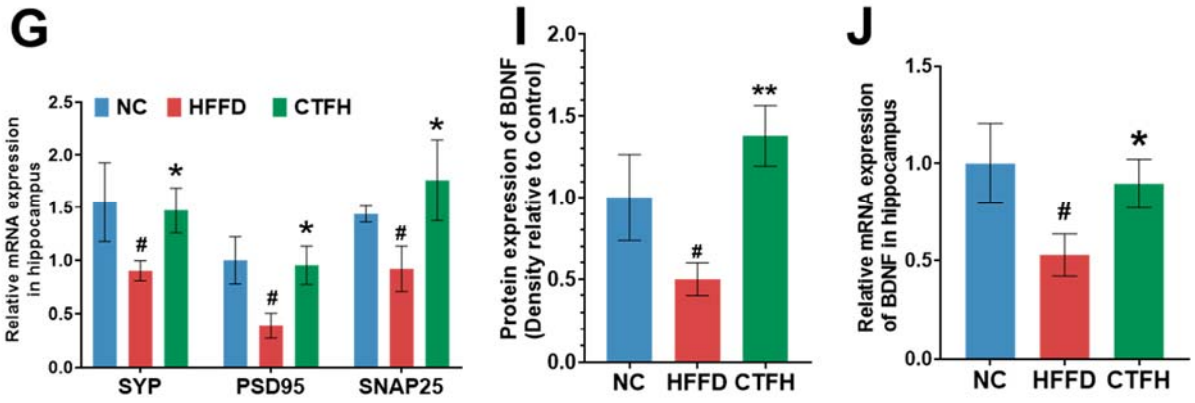

Fig. 3. CTF ameliorated synaptic plasticity and neurotrophic factors in the hippocampus. (A) Hippocampal sections stained with H&E staining at 500 μm and 200 μm; (B) Representative TEM of PSD (500 nm) (*n*=3); (C-D) The length and width of PSD (*n*=3); (E) Representative WB analysis of PSD95, SYP, and SNAP25 in mice hippocampus. (F) Quantification of PSD95, SYP, and SNAP25 protein levels; (G) Relative mRNA expression of hippocampal *Psd95, Syp*, and *Snap25*; (H) Representative WB analysis of hippocampal BDNF. (I) Quantification of BDNF protein levels; (J) Relative mRNA expression of hippocampal *Bdnf*. Data are presented as the mean ± SD (*n*=3). #$P < 0.05$, ##$P < 0.01$, ###$P < 0.001$ in comparison to the NC group; *$P < 0.05$, **$P < 0.01$, ***$P < 0.001$ in comparison to the HFFD group. *p*-values were calculated by one-way ANOVA with Tukey's or Tamhane's tests. Abbreviations: PSD, postsynaptic density; TEM, Transmission Electron Microscope; WB, Western Blotting; PSD95, Postsynaptic density protein-95; SYP, Synaptophysin; SNAP25, Synaptosome associated protein-25. BDNF, Brain-derived neurotrophic factor; H&E staining, hematoxylin-eosin staining.

Given the critical role of postsynaptic density (PSD) in synaptic transmission and cognitive processes (Pan et al., 2023), we next examined synaptic ultrastructure. TEM analysis showed PSD length (1.36-folds than HFFD group, $P < 0.05$) and thickness (1.89 folds than HFFD group, $P < 0.01$) were significantly increased in the CTFH group (Fig. 3B-D). Consistently, WB and qRT-PCR analyses revealed CTF upregulated the expression of PSD95, a key synaptic scaffold protein, in the hippocampus (Fig. 3E–G, $P < 0.05$). Additionally, CTF increased the levels of SNAP25 and SYP, two essential proteins involved in synaptic vesicle fusion and neurotransmitter release (Fig. 3E–G, $P < 0.05$), suggesting enhanced synaptic structural integrity. Moreover, BDNF directly facilitates axonal growth and enhances synaptic functional plasticity via promoting long-term potentiation (Wang et al., 2023). WB and qRT-PCR analysis illustrated CTF elevated BDNF accumulation in the hippocampus of HFFD mice (Fig. 3H-J, $P < 0.05$). These results fully validated the improvement effect of CTF on HFFD-induced synaptic structural and functional impairments in mice.

3.4. CTF significantly modulated serum tryptophan metabolic profiles.

To explore the systemic metabolic effects of CTF in HFFD-induced cognitive impairment, untargeted metabolomics was performed on serum samples. PCoA analysis characterized the overall changes in metabolic profiles (Fig. 4A). The score plots demonstrate tight clustering of quality control (QC) samples, confirming the stable reliability of LC-MS system during analysis. Altogether 1258 metabolites were detected in serum and were classified based on the HMDB database, among which 86 metabolites were identified as differentially expressed metabolites (DEMs) by multivariate statistical analysis in three groups. To explore the impacts of CTF on metabolic pathways in HFFD-fed mice, the serum DEMs were subjected to KEGG pathway analysis via MetaboAnalyst 5.0. The result showed Try metabolism was more significant in this

study (Pathway effect values ≥ 0.4), and notably, differential TRYs were marked in volcanic maps (Fig. 4B-E).

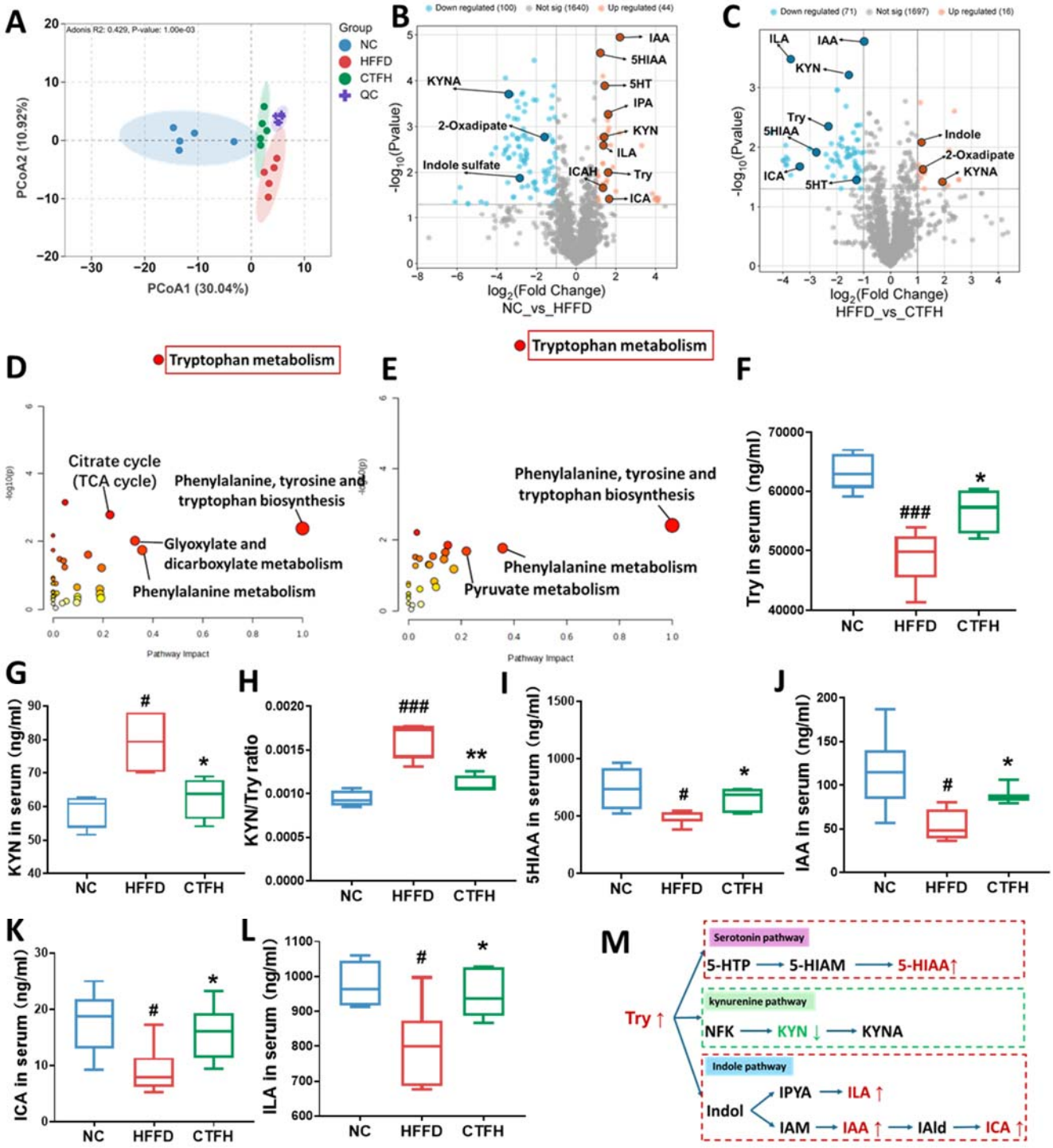

Fig. 4. CTF modulated tryptophan metabolic profiles in serum (n=5). (A) Principal coordinates analysis (PCoA) analysis; (B-C) Volcano plots depicting representative differentially TRYs between the NC group and HFFD group (B), and between the HFFD group and CTFH group (C); (D-E) KEGG pathway analysis using differential metabolites between the NC group and HFFD group (D), and between the HFFD group and CTFH group (E); (F) The concentration of Try in serum; (G) The concentration of KYN in serum; (H) The ratio of KYN/Try in serum; (I) The concentration of 5HIAA in serum; (J) The concentration of IAA in serum; (K) The concentration of ICA in serum; (L) The concentration of ILA in serum. (M) Try metabolism pathway. Data are presented as the mean ± SD. #$P < 0.05$, ##$P < 0.01$, ###$P < 0.001$ in comparison to the NC group, *$P < 0.05$, **$P < 0.01$, ***$P < 0.001$ in comparison to the HFFD group. p-values were calculated by one-way ANOVA with Tukey's or Tamhane's tests. Abbreviations: KYNA, kynurenic acid; KYN, L-kynurenine; IAA, indole-3-acetic acid; 5HIAA, 5-hydroxyindole-3-acetic acid; 5HT, 5-hydroxy-L-tryptophan; IPA, indole-3-pyruvic acid; ILA, indole-3-lactic

acid; ICAH, indole-3-carboxaldehyde; Try, L-tryptophan; ICA, indole-3-carboxylic acid; ICAH, indole-3-carboxaldehyde. TRYs, tryptophan metabolites; KEGG, Kyoto Encyclopedia of Genes and Genomes.

Given the central role of Try metabolism, targeted metabolomics was subsequently applied to quantify key TRYs in serum (Table S8). Additionally, the information about metabolites stability (RSD < 11%) during sample processing and storage conditions (4℃) were displayed in Table S9. Dietary Try is metabolized in the body through three pathways, including the serotonin pathway, the kynurenine (KYN) pathway and the intestinal bacteria-derived indole pathway (Xue et al., 2023). CTFH significantly increased levels of indole-3-acetic acid (IAA), 5-hydroxyindoleacetic acid (5-HIAA), indole-3-lactic acid (ILA), indole-3-carboxylic acid (ICA), and Try, while reducing KYN and the KYN/Try ratio (Fig. 4F–L, $P < 0.05$). As a result, a holistic serum Try metabolic network map was constructed (Fig. 4M), which indicated CTF administration increased gut microbiota derived Try metabolism to the serotonin and indole pathways but decreased it to the KYN pathway.

3.5. CTF partially restored normal gut microbiota composition and regulates microbiota-derived tryptophan metabolites.

To investigate the role of the gut microflora in Try metabolism for CTF administration, 16SrRNA sequencing was performed on the fecal samples. HFFD feeding significantly altered microbial α-diversity (ACE, Chao1, Shannon, Simpson indices; Fig. S2A–D, $P < 0.001$) and β-diversity (Bray–Curtis-based PCoA; Fig. S2E-F), which were partially restored by CTFH treatment. At the phylum level, HFFD increased *Firmicutes* and decreased *Bacteroidetes*, while CTFH reversed this trend (Fig. 5A). At the genus level, harmful bacteria *Faecalibaculum* was substantially higher in the HFFD group compared to the NC group, whereas probiotics *Allobaculum*, *Bacteroides*, *Clostridium*, *Roseburia*, *Akkermansia,* etc., were clearly lower (Fig. 5B), while the CTFH showed a relative increase in the above-mentioned beneficial bacteria and the relative reduction of *Faecalibaculum* in comparison to the HFFD group by LEfSe assessment (Fig. 5B-D). The cluster heatmap further confirmed CTFH-mediated remodeling of gut microbiota (Fig. 5E). Moreover, KEGG annotation-based PICRUSt analysis showed the Try metabolism was significantly enriched in the CTFH group (Fig. 5F), suggesting its critical role in CTF's protective mechanism of cognitive impairment. Next, Spearman correlation analysis between differential TRYs quantified using targeted metabolomics in serum and differentially expressed intestinal bacteria was conducted, showing that beneficial bacteria (*Roseburia, Oscillibacter, Colidextribacter*, etc.,) were positively correlated with Try, 5HIAA, IAA, ICA, and ILA, while harmful bacteria (*Dubosiella*) were negatively correlated with them (Fig 5G).

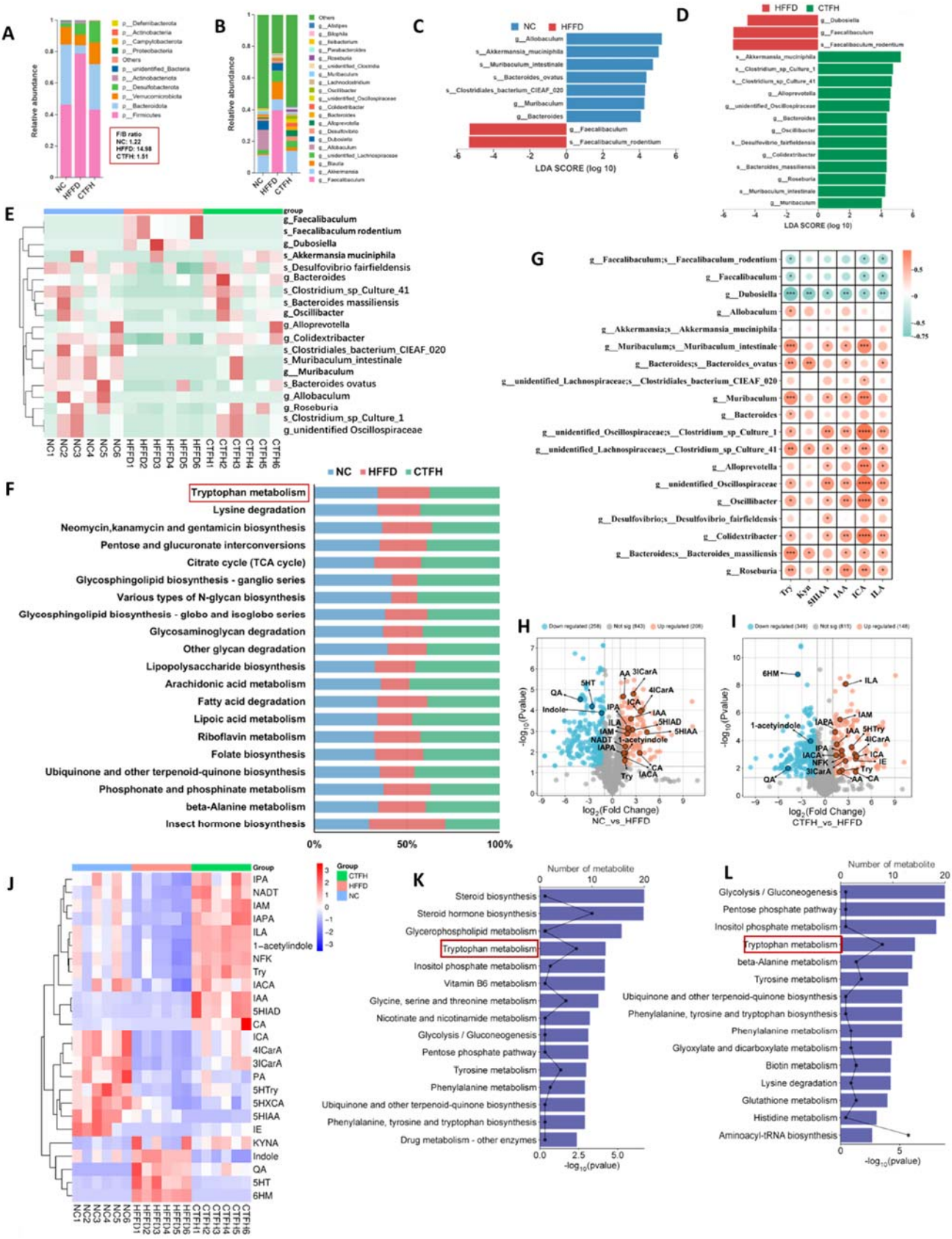
A
B
C
D
E
F
G
H
I
J
K
L
NC
HFFD
CTFH
LDA SCORE (log 10)
Relative abundance
F/B ratio
NC: 1.22
HFFD: 14.98
CTFH: 1.51
Tryptophan metabolism
Lysine degradation
Neomycin,kanamycin and gentamicin biosynthesis
Pentose and glucuronate interconversions
Citrate cycle (TCA cycle)
Glycosphingolipid biosynthesis - ganglio series
Various types of N-glycan biosynthesis
Glycosphingolipid biosynthesis - globo and isoglobo series
Glycosaminoglycan degradation
Other glycan degradation
Lipopolysaccharide biosynthesis
Arachidonic acid metabolism
Fatty acid degradation
Lipoic acid metabolism
Riboflavin metabolism
Folate biosynthesis
Ubiquinone and other terpenoid-quinone biosynthesis
Phosphonate and phosphinate metabolism
beta-Alanine metabolism
Insect hormone biosynthesis
0%
50%
100%
Number of metabolite
-log10(pvalue)
log2(Fold Change)
NC_vs_HFFD
CTFH_vs_HFFD
Steroid biosynthesis
Steroid hormone biosynthesis
Glycerophospholipid metabolism
Tryptophan metabolism
Inositol phosphate metabolism
Vitamin B6 metabolism
Glycine, serine and threonine metabolism
Nicotinate and nicotinamide metabolism
Glycolysis / Gluconeogenesis
Pentose phosphate pathway
Tyrosine metabolism
Phenylalanine metabolism
Ubiquinone and other terpenoid-quinone biosynthesis
Phenylalanine, tyrosine and tryptophan biosynthesis
Drug metabolism - other enzymes
Glycolysis / Gluconeogenesis
Pentose phosphate pathway
Inositol phosphate metabolism
Tryptophan metabolism
beta-Alanine metabolism
Tyrosine metabolism
Ubiquinone and other terpenoid-quinone biosynthesis
Phenylalanine, tyrosine and tryptophan biosynthesis
Phenylalanine metabolism
Glyoxylate and dicarboxylate metabolism
Biotin metabolism
Lysine degradation
Glutathione metabolism
Histidine metabolism
Aminoacyl-tRNA biosynthesis

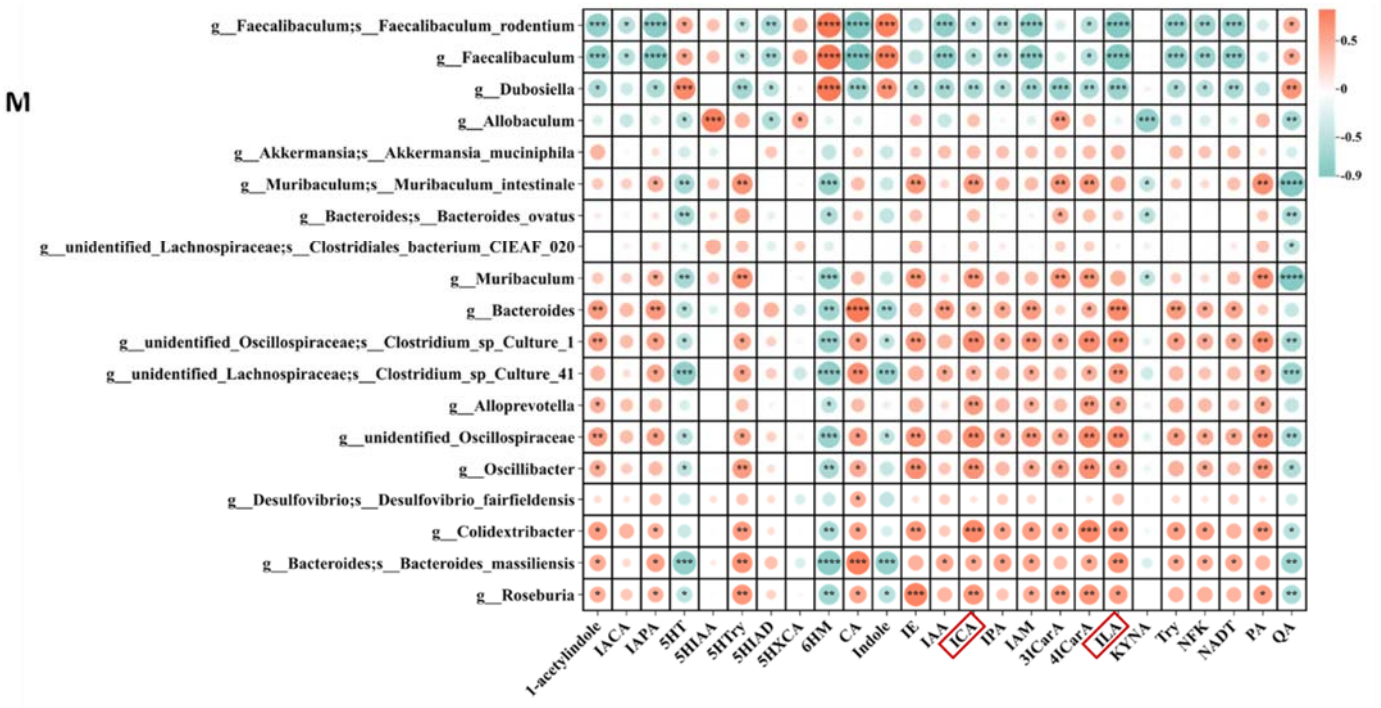

Fig. 5. CTF reshaped gut microbiota and microbial TRYs in cecal contents (n=6). (A) Relative abundance of differential gut microbiota at the phylum level; (B) Relative abundance of differential gut microbiota at the genus level. (C-D) Taxonomic cladogram obtained from LEfSe analysis of differential gut microbiota (LDA score > 4, $\alpha < 0.1$); (E) Heatmap of differentially expressed intestinal bacteria; (F) Prediction of KEGG metabolic pathways in microbial communities using PICRUSt; (G) A two-tailed Spearman correlation heatmap demonstrating the correlation between bacterial abundance that differs from other groups at the genus level and differential TRYs quantified using targeted metabolomics in serum, with positive correlations in red and negative correlations in blue (*$P < 0.05$, p**<0.01, and p***<0.001). (H-I) Volcano plots depicting representative differentially TRYs between the NC group and HFFD group (H), and between the HFFD group and CTFH group (I); (J) A heatmap showing potential differential TRYs in feces in different groups; (K-L) KEGG pathway analysis using differential metabolites between the NC group and HFFD group (K), and between the HFFD group and CTFH group (L); (M) A two-tailed Spearman correlation heatmap showing the correlation coefficient between bacterial abundance that differs from other groups at the genus level and differential TRYs levels in feces, with positive correlations in red and negative correlations in blue (*$P < 0.05$, p**<0.01, and p***<0.001). Abbreviations: KYNA, kynurenic acid; KYN, L-kynurenine; IAA, indole-3-acetic acid; 5HIAA, 5-hydroxyindole-3-acetic acid; 5HT, 5-hydroxy-L-tryptophan; IPA, indole-3-pyruvic acid; ILA, indole-3-lactic acid; ICAH, indole-3-carboxaldehyde; Try, L-tryptophan; ICA, indole-3-carboxylic acid; ICAH, indole-3-carboxaldehyde; QA, quinolinic acid; IAM; indole-3-acetamide; 5HIAD, 5-hydroxyindole acetaldehyde; IACA, 3-indoleacrylic acid; IAPA, 3-indolepropionic acid; 4IcarA, indole-4-carboxaldehyde; 5HIAD, 5-hydroxyindole acetaldehyde; NADT, N-acetyl-D-tryptophan; NFK, *N*'-formylkynurenine; IAPA, 3-indolepropionic acid; IE, indole 3-ethanol; 5HTry, 5-hydroxytryptophol; 6HM, 6-hydroxymelatonin.

To assess the effect of CTFH on intestinal microbiota metabolites, widely targeted metabolic profiling of the cecal contents was conducted and revealed 1,438 metabolites, with clear group separation in PCA (Fig. S2F). A total of 260 DEMs (VIP > 1, $P < 0.05$, |FC| > 2) were identified, including 20 tryptophan-related compounds (Fig. 5H–I). HFFD reduced total TRYs (indole pathway), which were significantly restored by CTFH (Fig. 5J). In addition, the metabolite set enrichment analysis (MSEA) also confirmed that Try metabolism was significantly enriched in both NC *vs*. HFFD and CTFH *vs.* HFFD comparisons (Fig 5K-L). Finally, Spearman correlation analysis between intestinal bacteria-derived TRYs in feces and differentially expressed intestinal bacteria was performed, illustrating beneficial bacteria (*Roseburia Oscillibacter, Colidextribacter, etc.,*) were positively correlated with TRYs (especially ICA, and ILA), while harmful bacteria (*Dubosiella*) were negatively correlated with them (Fig 5M).

3.6. CTF promoted hippocampal TRYs production and increased AHR expression in hippocampal tissue.

Studies have shown that certain gut-derived TRYs can cross the BBB and have neuroprotective effects (Xue et al., 2023). Our results consistently showed that CTF significantly increased hippocampal levels of Try ($P < 0.001$), ICA ($P < 0.05$), and ILA ($P < 0.05$) compared to the HFFD group, partially restoring them to normal levels (Fig. 6A–C). These findings suggest that ICA and ILA, two microbiota-derived indole derivatives, may cross the BBB and contribute to neuroprotection. Given that indoles are endogenous ligands of the AHR, we next assessed AHR expression in the hippocampus. Immunofluorescence analysis revealed a lower AHR expression in HFFD mice comparable to the NC group ($P < 0.01$), while the CTFH group demonstrated markedly higher AHR expression ($P < 0.05$) (Fig. 6D–E). This result was further validated by qRT-PCR (Fig. 6F). These results imply that the neuroprotective effect of CTF may correlate with the increased AHR expression in the brain.

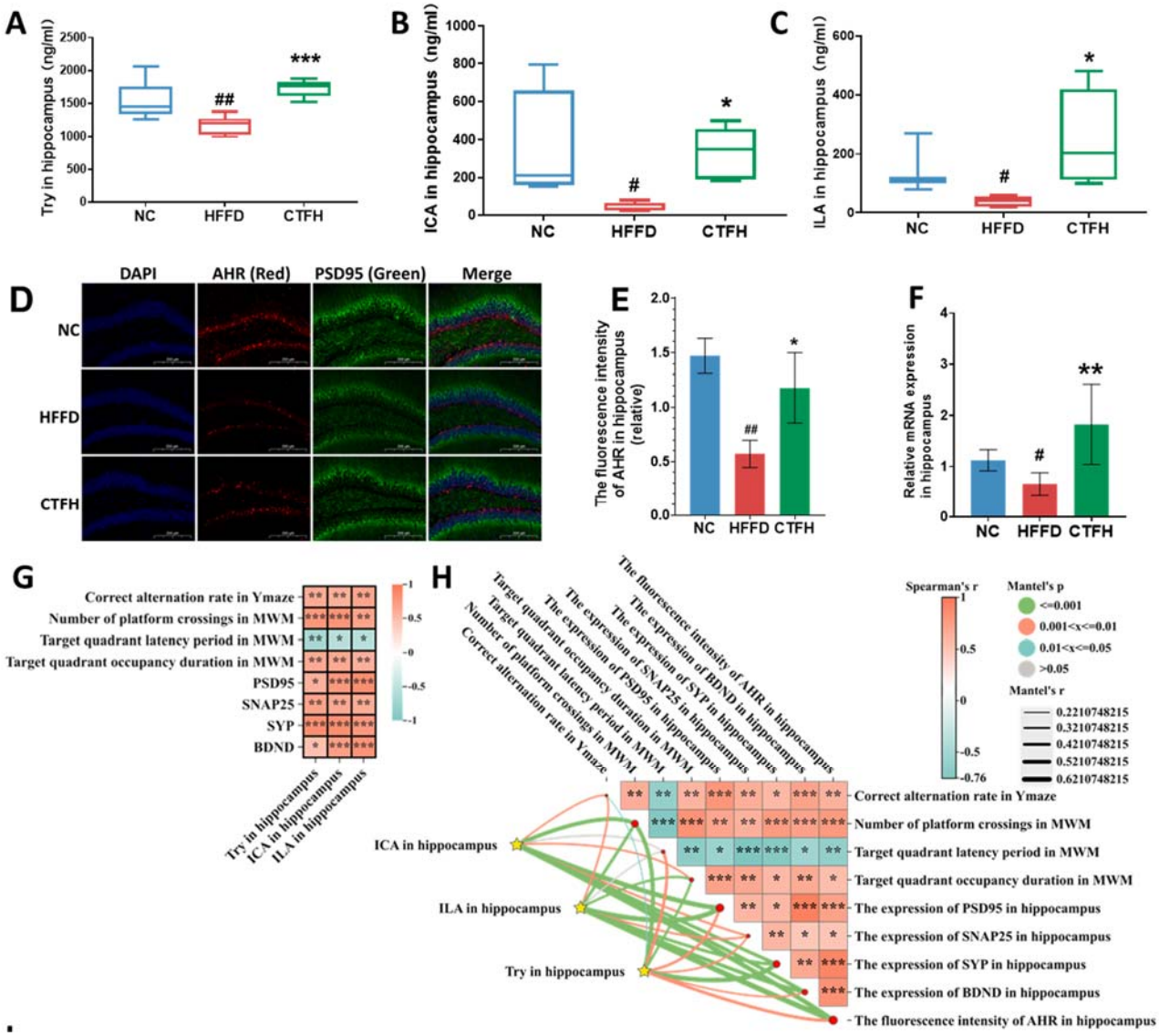

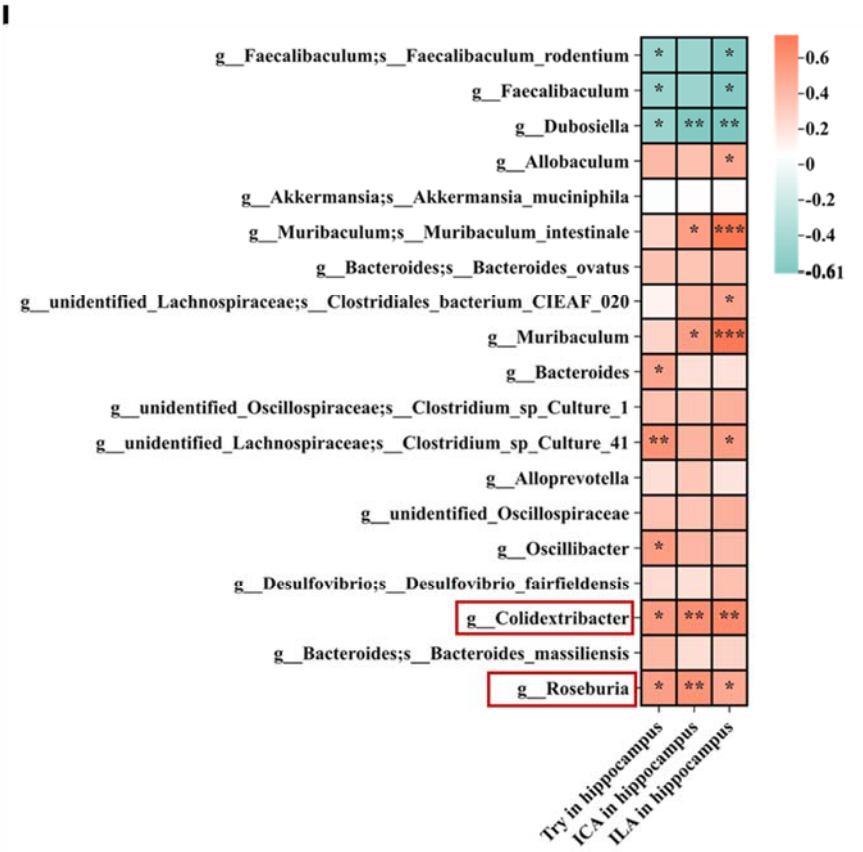

Fig. 6. CTF promoted hippocampal TRYs production and activated AHR expression in hippocampal tissue. (A) Hippocampal Try levels; (B) Hippocampal ICA levels; (C) Hippocampal ILA levels; (D) co-immunofluorescence image of AHR and PSD95 in hippocampus (500 μm), stained for PSD95 (green), AHR (red) and DAPI (blue). (E) Quantification of AHR in the hippocampus. (F) Relative mRNA expression of *Ahr* in mice hippocampus; (G) Heatmap of the correlation between the cognitive impairment phenotype and TRYs in hippocampus. (H) Pairwise comparisons of cognitive phenotypes are shown, with a color gradient denoting Spearman's correlation coefficient. Try, ILA, ICA were related to each cognitive factor by partial Mantel tests. Edge width is proportional to the Mantel's *r* statistic for the respective distance correlations, while edge color indicates statistical significance. (I) Correlations between the levels of Try, ILA, ICA, and the significantly differing relative abundance of bacteria at the genus levels. Data are presented as the mean ± SD. #$P < 0.05$, ##$P < 0.01$, ###$P < 0.001$ in comparison to the NC group, *$P < 0.05$, **$P < 0.01$, ***$P < 0.001$ in comparison to the HFFD group. *p*-values were calculated by one-way ANOVA with Tukey's or Tamhane's tests. Abbreviation: ICA, indole-3-carboxylic acid; ILA, indole-3-lactic acid.

To explore the functional significance of these metabolites, we performed correlation analyses between hippocampal Try and TRYs (ICA and ILA) and cognitive performance metrics, including MWM (platform crossings, quadrant duration, latency) and Y-maze (alternation rate), synaptic and neurotrophic markers (PSD95, SYP, SNAP25, BDNF), and AHR in the hippocampus. Spearman and Mantel tests showed that hippocampal ILA and ICA were positively associated with behavioral performance and expression of these markers but negatively correlated with MWM latency (Fig. 6G–H). Moreover, Spearman analysis revealed that ICA and IAA levels showed a positive correlation with the abundance of *Roseburia* and *Colidextribacter*, indicating these bacteria may contribute to CTF-mediated regulation of TRY metabolism and brain function (Fig. 6I).

These results suggest that CTF ameliorates HFFD-induced disruption of gut microbiota-related Try metabolism. By promoting the production and brain entry of indole metabolites (ILA and ICA), CTF

enhanced synaptic and neurotrophic function and was associated with activation of AHR signaling, thereby exerting cognitive protective effects.

3.7. The depletion of gut microbiota diminishes CTF-mediated protection against HFFD-related cognitive deficits.

To determine whether the intestinal microbiota mediates the cognitive benefits of CTF, mice fed with HFFD were pretreated with a wide-spectrum ABX to eliminate gut microbiota preceding CTF administration. 16S rRNA sequencing of cecal contents confirmed that ABX treatment markedly reduced both α and *β* diversity, with a sharp increase in *Proteobacteria* abundance (Fig. S3A–G), indicating effective microbiota depletion in the AB and AC groups.

The OFT assay revealed no significant difference in the 5-minute travel distance among groups (Fig. 7A). The MWM test showed ABX treatment significantly reduced CTF-mediated cognitive decline in HFFD mice, evidenced by longer escape latency ($P < 0.05$), shorter target quadrant time ($P < 0.05$), and fewer platform crossings ($P < 0.05$) (Fig. 7B-E). The trajectory diagram of the water maze is shown in Fig. S3H. The Y maze test further indicated that ABX treatment decreased 30.46% the spontaneous alternation percentage in CTF-intervened mice (Fig. 7F, $P < 0.01$). TEM analysis of PSD also revealed that antibiotic treatment decreased hippocampal postsynaptic density in CTFH mice (Fig. 7G-I, $P < 0.05$). Of note, the concentration of Try, ICA and ILA in the hippocampus, serum, and feces reduced in AC groups compared to the CTFH group (Fig. 7J-O; Fig. S3I-J, $P < 0.05$). Collectively, these findings indicate that the protective effect of CTF against HFFD-induced cognitive disorder relies on the gut microbiome.

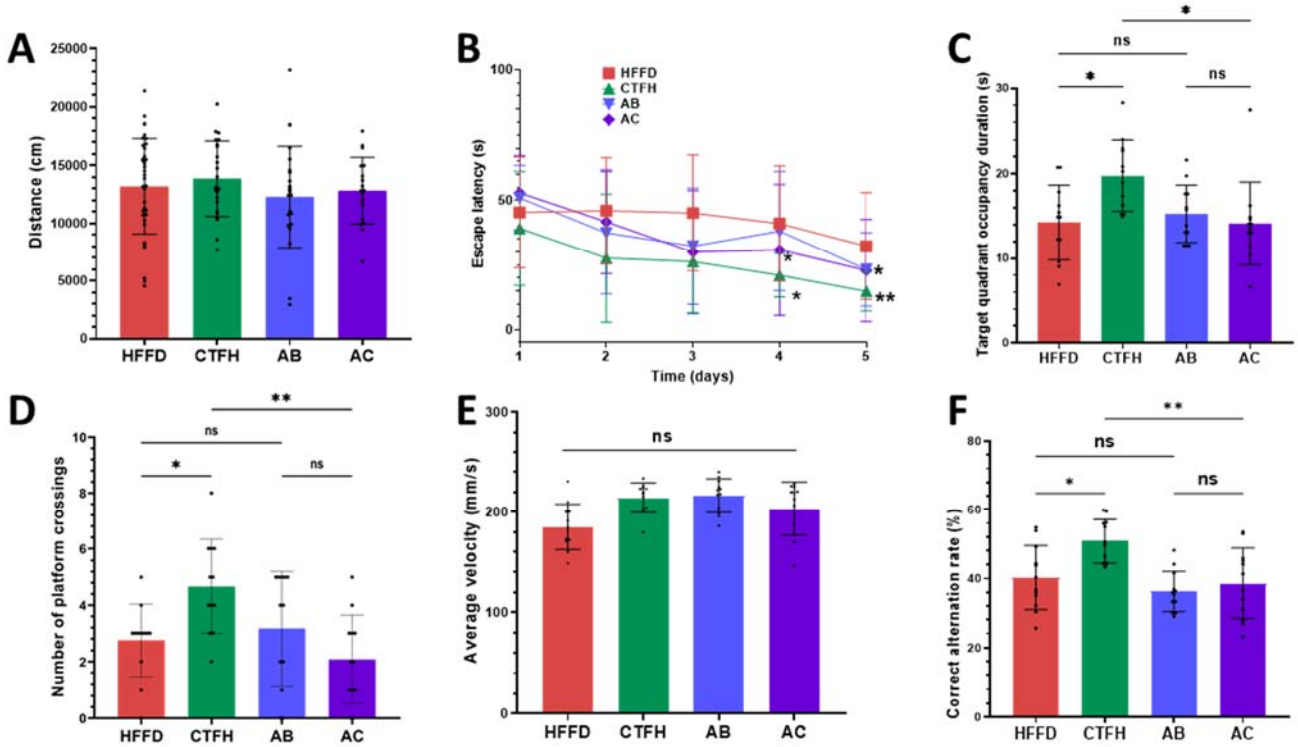

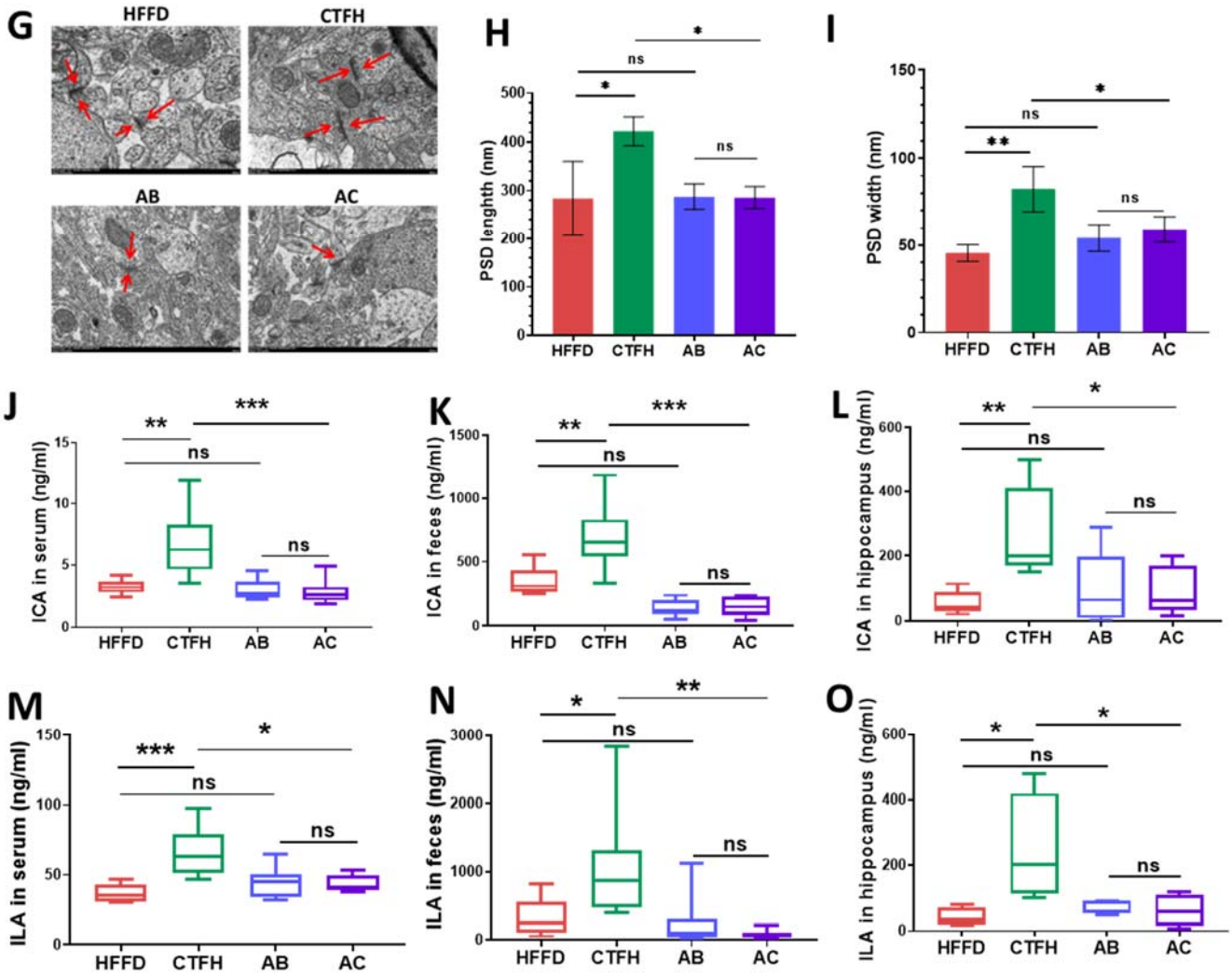

Fig. 7. The gut microbiota plays a crucial role in the beneficial effects of CTF for improving cognitive impairment. (A) Distance for 5 min in OFT; (B) Escape latency during the place navigation test in MWM; (C-E) Escape latency, time spent in the target quadrant, number of platform crossings, average swimming speed, (F) Spontaneous alternation in the Y-maze test; (G) Representative TEM of PSD (500 nm) (n=3); (H-I) The length and width of PSD (n = 3). (J-L) Concentration of ICA in serum, feces, and hippocampus; (M-O) Concentration of ILA in serum, feces, and hippocampus. Data are presented as the mean ± SD. *P < 0.05, **P < 0.01, ***P < 0.01. p values were calculated by one-way ANOVA with Tukey's or Tamhane's tests. Abbreviation: ICA, indole-3-carboxylic acid; ILA, indole-3-lactic acid.

3.8. ILA and ICA mitigated synaptic damage in SH-SY5Y cells induced by HG

To confirm the contributions of ILA and ICA to neural synapses, we first established the high-glucose (HG) injury model in SH-SY5Y cells. Screening for optimal HG conditions showed that treatment with 75 mM glucose for 24h resulted in a significant reduction in cell viability compared to the control group (P < 0.05, ;Fig. 8A), which is consistent with previouse reseach (Li et al., 2024). Thus, 75 mM concentration was subsequently used for all HG induction studies. Furthermore, the cytotoxicity of ILA and ICA was evaluated, confirming that neither metabolite induced toxic effects on SH-SY5Y cells at doses below 80 μM (P < 0.05; Fig. 8B-C). Subsequently, we treated SH-SY5Y cells with 75 mM D-glucose (HG) and 10-40 μM ICA or ILA, respectively. According to the results of cell viability assays, 40 μM and 20 μM were the optimal concentrations of ICA and ILA, respectively, in this study (P < 0.05; Fig. 8D-E).

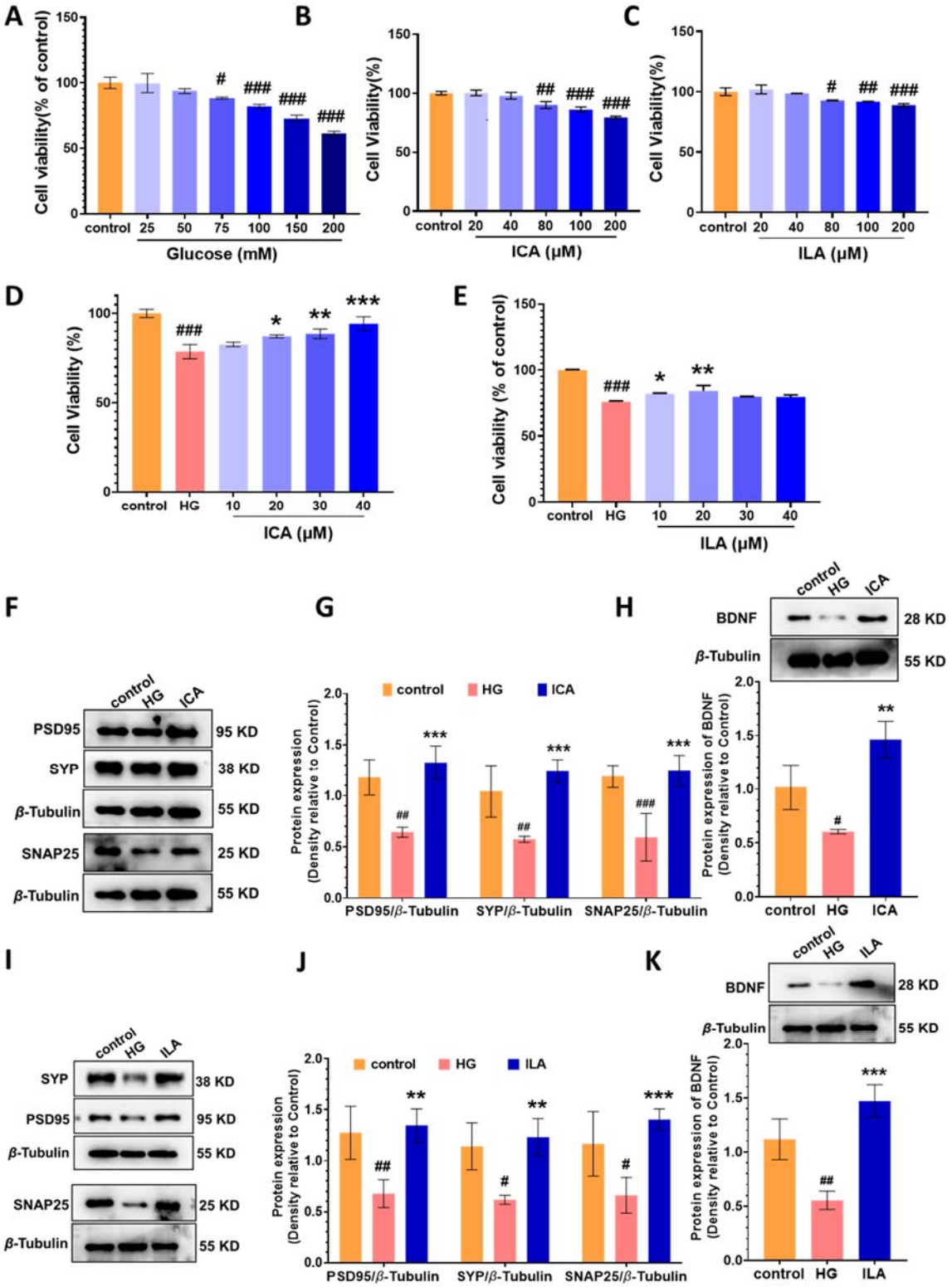

Fig. 8. ILA and ICA improved HG (high glucose)-induced synaptic damage. (A) SH-SY5Y neuroblastoma cells viability was assessed were using the CCK8 assay, which were treated with 25-200 mM D-glucose for 48 h. (B-C) SH-SY5Y neuroblastoma cells viability was assessed were using the CCK8 assay, which were treated with 20-200 mM ICA or ILA for 48 h. (D-E) SH-SY5Y neuroblastoma cells viability was assessed were using the CCK8 assay, which were treated with 75 mM D-glucose and with 0-40 μM ICA or ILA for 48 h. (F-G) Representative WB analysis and quantification of PSD95, SYP, and SNAP25 in SH-SY5Y cells treated by 75 mM D-glucose and 40 μM ICA for 48 h. (H) Representative WB analysis and quantification of BDNF in SH-SY5Y cells treated by 75 mM D-glucose and 20 μM ICA for 48 h. (I-J) Representative WB analysis and quantification of PSD95, SYP, and SNAP25 in SH-SY5Y cells treated by 75 mM D-glucose and 20 μM ILA for 48 h. (K) Representative WB analysis and quantification of BDNF in SH-SY5Y cells treated by 75 mM D-glucose and 20 μM ILA for 48 h. Data are presented as the mean ± SD. #$P < 0.05$, ##$P < 0.01$, ###$P < 0.001$ in comparison to the Control group, *$P < 0.05$, **$P < 0.01$, ***$P < 0.001$ in comparison to the HG group. p-values were calculated by one-way ANOVA with Tukey's or Tamhane's tests.

To evaluate the effects of ICA and ILA on synaptic plasticity, we measured HG-induced PSD95, SYP, SNAP-25, and BDNF protein expression in SH-SY5Y cells. In Fig. 8F-K, SH-SY5Y cells maintained in HG showed significant reductions in expression levels of PSD95, SYP, SNAP-25, and BDNF when compared with control group cells ($P < 0.05$). However, treatment with 40 μM ICA or 20 μM ILA increased the expression of synapse-associated proteins and neurotrophic factors ($P < 0.01$; Fig. 8F-K). Accordingly, ICA or ILA could upregulate synaptic plasticity HG-induced SH-SY5Y cells.

4. Discussion

Coreopsis tinctoria (CTF) has a history of consumption as a herbal (Wang et al., 2017) tea in traditional practices, suggesting its likely safety for short-term human use at dietary-relevant doses (Liu et al., 2023). Aierken et al. (2018) did not find any genetic toxicity in CTF through Ames test, mammalian cell chromosome aberration test *in vitro,* micronucleus test, sperm abnormality test, and mouse spermatogonial or spermatocyte chromosome aberration test. However, it must be clearly stated that systematic clinical trials to establish the safety, tolerability, and appropriate dosage of standardized CTF extracts for therapeutic purposes in humans are still lacking. Such investigations represent an indispensable and crucial step before any clinical application can be considered.

HFFD feeding induced obesity and glucose metabolic dysfunction, known risk factors for neurodegenerative disease (Sun et al., 2022). Earlier research showed that the CTF extract and its bioactive compounds exhibit neuroprotective effects in cell culture and in animal models by influencing factors related to neuroinflammation, alleviating oxidative stress, and enhancing acetylcholine, as well as altering intestinal microbiota (Shen et al., 2021). Nevertheless, the role of intestinal microflora in the effect of CTF on HFFD-induced cognitive impairment remains largely not understood.

In this study, HFFD-fed mice exhibited significant deficits in spatial and working memory, accompanied by gut microbiota dysbiosis and impaired Try metabolism, characterized by reduced levels of key microbial-derived metabolites such as ILA and ICA. However, oral administration of CTF (100-400 mg/kg/day) could reverse the cognitive behavior changes and promote Try and intestinal bacteria-derived TRYs production, especially ILA and ICA. More importantly, the protective effects of ICA and ILA on synaptic damage have been confirmed in SH-SY5Y cells. As both ILA and ICA are known ligands of the AHR, further analyses revealed that CTF treatment was related to increased hippocampal expression of AHR and BDNF, together with elevated levels of synaptic plasticity markers including PSD95, SNAP25 and SYP. These findings indicate that the cognitive benefits of CTF may be mediated through modulation of the gut microbiota–Try–brain axis, ultimately supporting synaptic function and neuronal plasticity in the context of HFFD-induced cognitive impairment.

A thorough investigation of plant-derived products and metabolites is necessary for understanding the intricacies of natural food therapy (Han et al., 2025). The bioactivity of CTF is predominantly attributed to its polyphenolic compounds (Gao et al., 2025). However, the insufficient characterization of these phenolics in CTF poses a major obstacle to advancing bioactivity studies of plant-derived beverages. FBMN, an emerging

mass spectrometry technique, provides notable advantages for isomer and stereoisomer discrimination by integrating the excellent separation capabilities of liquid chromatography with the robust characterization power of mass spectrometry (Nothias et al., 2020). However, FBMN also has limitations in distinguishing isomers, especially lacks isomers standard compounds and public database support, which leads to a decrease in the confidence level of annotations (Li et al., 2022). Natural medicines typically exhibit a complex material basis, and systematic research approaches for this remain underdeveloped, often failing to yield reliable data on their active ingredients (Han et al., 2025). Another challenge of FBMN is the separation of different ion adducts (such as protonation and sodiation), which leads to redundant subnetworks and indirectly affects isomer recognition (Schmid et al., 2021). Thus, multi-layer validation strategies are required in FBMN analysis. Currently, the strategy of LC-MS/MS-based FBMN technology was employed to comprehensively detect phytochemicals in CTF, with 178 compounds being comprehensively characterized and, among them, 57 constitutions being first reported (Fig. 1 and Table S5). Of note, some quinic acid and flavonoid derivatives with similar fragmentation patterns and molecular structure in CTF were found and annotated through FBMN (Fig. 1 and Table S5). Moreover, considering safety and environmental protection, an environmentally friendly extraction of an ethanol-water mixture was selected as a solvent to extract active ingredients in CTF. The extract preparation removes ethanol via concentration, and the final freeze-dried product for animal feeding is ethanol-free, posing no harm in practical food applications.

Dysregulation of Try metabolism has emerged as a key contributor to the gut–brain axis and is increasingly recognized for its role in cognitive impairment and neurodegenerative diseases (Li et al., 2024). Dietary Try is metabolized through three primary pathways: first, the gut microbial indole pathway, yielding neuroactive metabolites such as ILA, ICA, IAA, IPA, etc.; second, the KYN pathway in immune and epithelial cells, generating metabolites such as quinolinic acid (QUIN), which has neurotoxic potential; and third, the serotonin (5-HT) pathway in enterochromaffin cells, producing neuroactive amines (Xue et al., 2023). Among these, indole derivatives have shown potent neuroprotective properties, and recent studies indicate that plant polyphenols may influence these metabolic routes by reshaping gut microbial composition. For instance, a polyphenol, quinic acid, derived from millet, significantly increased gut microbial TRYs (IAA), inhibiting the DR3/IKK/NF-κB signaling to mitigate oxidative stress and neuroinflammation in HFD-exposed brains (Li et al., 2024). In the present study, serum metabolomics illustrated an elevation in Try, 5HIAA, IAA, ILA, and ICA levels and a decrease in KYN concentrations with CTF, showing that Try metabolism transitioned from the KYN pathway to the 5-HT and indole pathways (Fig. 4). A study reported that the blood levels of KYN and QA, along with the KYN/Try ratio, positively correlate with cognitive function in AD patients (Xue et al., 2023b). Consistently, the serum KYN/Try ratio was markedly higher in the HFFD group; however, CTF administration reversed this situation in our study (Fig. 4). Consistent with our results, accumulating evidence demonstrating that these microbially-derived tryptophan metabolites are absorbable, can be detected in systemic circulation (blood, urine, feces, cerebrospinal fluid, et al.) (Sun et al., 2022). Several structurally related indole derivatives (IPA, ILA, ICA, et al.) have been confirmed to exhibit

neuroactive properties, likely through direct access to the central nervous system (Hao et al., 2025; Jiang et al., 2024; Shang et al., 2025; Yin et al., 2023), which may means that these metabolites have high bioavailability. More importantly, only a relatively high concentration of ILA and ICA was detected in the hippocampus after CTF administration and significantly positively correlated with the indicators of cognitive improvement (Fig. 6G-H), indicating these two indoles could be indeed the key metabolites for CTF to improve HFFD induced cognitive impairment.

To date, several probiotic strains with the capability to synthesize TRYs and confer neuroprotective effects have been validated *in vivo* experimentally. A team reported *Roseburia* administration raised levels of 5-HT in the brain and colon but markedly decreased KYN and QUIN levels to ameliorate the mouse depressive behaviors (Zhou et al., 2023). Likewise, *Akkermansia_muciniphila* promoted 5-HT production and inhibited KYN production to reduce neuroinflammation (Jiang et al., 2024). The synbiotic *Clostridium sporogenes* and xylan could raise IPA production to enhance cognitive ability and spatial memory capacity in AD mice (Li et al., 2024). In our study, *Akkermansia_muciniphila, Muribaculum,* and *Bacteroides* were the common characteristic bacteria in the NC and CTFH groups compared with the HFFD group, whereas *Clostridium, Alloprevotella, Roseburia, Oscillibacter,* and *Colidextribacter* were the characteristic bacteria in the CTFH group (Fig. 5). Among them, *Colidextribacter* and *Roseburia* had the strongest correlation with hippocampal Try, ILA and ICA (Fig. 6I) and exhibited a positive association with cognitive improvement phenotype (Fig. 6G-H), indicating *Colidextribacter* and *Roseburia* might serve as the keystone bacteria in reaction to CTF administration. However, there are very limited direct studies on *Colidextribacter*, and its classification and function have not been fully clarified. Moreover, a pivotal consideration for the clinical translation of our findings is the well-documented inter-individual variation in gut microbiota composition. Indeed, our data demonstrate that the microbiota signature, particularly the baseline abundance of taxa capable of converting dietary tryptophan into ILA and ICA (e.g., *Colidextribacter* and *Roseburia* species), may serve as a key determinant and predictive biomarker for treatment responsiveness of cognitive impairment. Future clinical studies could explore strategies such as pre-screening for favorable microbial biomarkers or the co-administration of CTF with specific probiotic strains to ensure consistent and robust production of beneficial metabolites across diverse human populations.

AHR mediates immune regulation via indoles (as its ligands), benefiting neurological disorder (Sun et al., 2022). Activation of AHR has been linked to attenuation of neuroinflammation, astrocyte modulation, and enhancement of synaptic plasticity through upregulation of BDNF and synaptic proteins such as PSD95 (Ahmed et al., 2022). In our study, the hippocampal AHR expression level in HFFD group showed significantly lower levels than the NC and CTFH groups (Fig. 6D-F). Consistent with our findings, Postmortem brains of AD patients showed abnormal AHR levels versus normal controls (Ramos-García et al., 2020). Recently, researchers found that indole induces the expression of SYP and PSD95 in the hippocampus, with AHR being crucial for indole's neurogenic effects, as indole failed to promote neurogenesis in AHR KO mouse neutrospheres cultured *in vitro,* contributing to the number of DCX^+ cells in the hippocampal dentate

gyrus of indole-treated AHR KO mice being lower than that in wild-type mice (Wei et al., 2021). Analogously, the anti-inflammatory effect of indole-3-carbinol on microglia was reversed by AHR knockdown (Khan & Langmann, 2020). Research has shown that the action of AHR agonists is related to cytochrome P450 enzymes, which means, as established AHR agonists, ILA and ICA are likely to induce the expression of cytochrome P450 enzymes, particularly members of the CYP1A family (e.g., CYP1A1 and CYP1A2) (Xue et al., 2023). This raises a legitimate theoretical concern that concurrent use of indoles with medications that are substrates of these enzymes (e.g., clozapine, olanzapine, theophylline, and warfarin) could accelerate their metabolism, potentially reducing their clinical efficacy. Therefore, investigating the interaction potential of indole with commonly prescribed drugs must be an integral component of its future safety assessment. Any future clinical application should include clear communication of this potential interaction and may require monitoring of relevant drug levels in co-medicated individuals. Overall, as prospective mediators of the microbiota-gut-brain axis, indoles play a critical role in extenuating neurological disease. However, further investigation could be conducted to enable a comprehensive understanding of potential mechanisms for CTF against cognitive dysfunction.

5. Limitations and future prospects

While our study demonstrates some evidence supporting the potential of CTF in daily healthcare and clinical applications regarding its cognitive improvement effect, several limitations should be acknowledged. A notable limitation of this study is that antibiotics may impair the absorption and bioavailability of CTF extract. As Luo et al. (2024) demonstrated, broad-spectrum antibiotics disrupt gut microbiota, inhibiting β-glucosidase activity critical for converting flavonoid glycosides (e.g., curcumin) in the extract into absorbable aglycones. Liu et al. (2019) found antibiotics interference reduces plasma exposure of herbal components by 16.9%–50.9% and indicated a potential clinical drug-drug interaction (DDI) when herbal components were administered with broad-spectrum antibiotics. Therefore, future research should exclude the impact of antibiotic administration reducing the absorption and bioavailability of active ingredients in CTF, which leads to a decrease in pharmacological activity. Additionally, in our experiment, CTF was preventively administered to HFFD-fed mice. Due to the unclear pathogenesis of HFFD-induced cognitive impairment, it is still unclear whether CTF alleviates cognitive impairment by blocking HFFD-induced metabolism disorders or simultaneously alleviates glucolipid metabolism disorders and cognitive impairment. Therefore, the therapeutic effect of CTF should be evaluated in the future to eliminate the possibility that CTF may prevent cognitive impairment by firstly addressing lipid metabolism disorders. Furthermore, although quantitative analysis of CTF components identified marein as a major polyphenol, whether this specific compound is essential for preventing HFFD-induced diseases requires further clarification. Additionally, From the microbiota–gut–brain axis perspective, the mechanisms by which gut microbiota and diet-associated TRYs influence neuroinflammation and cognitive impairment remain unclear. Elucidating the specific molecular targets of CTF action also presents an ongoing challenge. Moreover, further research is essential to clarify the role of gut microbiota in CTF-mediated cognitive improvement observed in animal studies, including fecal

microbiota transplantation, single bacterium colonization assessment (specific bacterial strains), further functional verification of alone administration of ILA or ICA *in vivo*, toxicological testing, and controlled human intervention trials.

6. Conclusion

In summary, this investigation provides novel insights into the phytochemical composition and gut–brain regulatory potential of CTF. The dietary supplementation of CTF could effectively improve HFFD-induced impairments in spatial learning and memory, accompanied by enhanced synaptic plasticity and increased BDNF expression in the hippocampus. These beneficial effects appear to be mediated, at least in part, through modulating gut microbiota and Try metabolism. Specifically, CTF treatment alleviated gut dysbiosis and Try metabolic disturbances, with *Roseburia* and *Colidextribacter* identified as potentially beneficial taxa, and indole derivatives such as ILA and ICA emerging as key neuroactive metabolites. However, the mechanism by which specific genes alter the gut microbiota and metabolites is unclear, and future studies are needed. Our study demonstrated that CTF promises to be a potential nutritional therapy for addressing HFFD-educed cognitive dysfunction, which provides a rationale for further application of edible CTF for preventing and alleviating neurodegenerative diseases in humans.

Declaration of competing interest

The authors declare that they have no known competing financial interests or personal relationships that could have appeared to influence the work reported in this paper.

Data availability

The data that has been used is confidential. All raw data can be obtained availability.

Funding

This research was financially supported by the specific research fund of CAMS Innovation Fund for Medical Sciences (Grant number: 2022-I2M-2-002), the National Natural Science Foundation of China (Grant number: 82174046) and The Innovation Platform for Academicians of Hainan Province.

Reference

Agustí, A., García-Pardo, M. P., López-Almela, I., Campillo, I., Maes, M., Romaní-Pérez, M., & Sanz, Y. (2018). Interplay Between the Gut-Brain Axis, Obesity and Cognitive Function. *Frontiers in Neuroscience*, *12*, 155. https://doi.org/10.3389/fnins.2018.00155

Ahmed, H., Leyrolle, Q., Koistinen, V., Kärkkäinen, O., Layé, S., Delzenne, N., & Hanhineva, K. (2022). Microbiota-derived metabolites as drivers of gut-brain communication. *Gut Microbes*, *14*(1), 2102878. https://doi.org/10.1080/19490976.2022.2102878

Aierken, T., Huang, R., Liu, X., & Xiong, J. (2018). Study on genotoxicity of <i>Coreopsis tinctoria<i> Nutt．. *Chinese Journal of Food Hygiene*, *30*(01). https://doi.org/10.13590/j.cjfh.2018.01.004

Christ, A., Lauterbach, M., & Latz, E. (2019). Western Diet and the Immune System: An Inflammatory Connection. *Immunity*, *51*(5), 794–811. https://doi.org/10.1016/j.immuni.2019.09.020

Dalile, B., Kim, C., Challinor, A., Geurts, L., Gibney, E. R., Galdos, M. V., La Fata, G., Layé, S., Mathers, J. C., Vauzour, D., Verkuyl, J. M., & Thuret, S. (2022). The EAT-Lancet reference diet and cognitive function across the life course. *The Lancet. Planetary Health*, *6*(9), e749–e759. https://doi.org/10.1016/S2542-5196(22)00123-1

Desmons, A., Humbert, L., Eguether, T., Krasniqi, P., Rainteau, D., Mahdi, T., Kapel, N., & Lamazière, A. (2022). High performance liquid chromatography–tandem mass spectrometry quantification of tryptophan metabolites in human serum and stool – Application to clinical cohorts in Inflammatory Bowel Diseases. *Journal of Chromatography A*, *1685*, 463602. https://doi.org/10.1016/j.chroma.2022.463602

Gao, S., Li, T., Li, Z.-R., Liao, B., Zhao, M., Zhou, C., Luo, D., & Jia, R.-B. (2025). Gradient ethanol extracts of *Coreopsis tinctoria* buds: Chemical and in vitro fermentation characteristics. *Food Chemistry*, *464*, 141894. https://doi.org/10.1016/j.foodchem.2024.141894

Guo, F., Abulati, A., Wang, J.-W., Jiang, J., Zhang, W.-X., Chen, P.-D., Yao, L., & Mao, X.-M. (2022). Flavonoids of *Coreopsis tinctoria* Nutt alleviate the oxidative stress and inflammation of glomerular mesangial cells in diabetic nephropathy via RhoA/ROCK signaling. *Journal of Functional Foods*, *89*, 104955. https://doi.org/10.1016/j.jff.2022.104955

Han, M., Xia, H., Xia, G., Wei, X., Li, J., Wu, Y., & Lin, S. (2025). Feature-based molecular networking (FBMN): An efficient booster for discovering novel natural products or metabolites. *Acta Pharmaceutica Sinica B*, *15*(4), 2283–2286. https://doi.org/10.1016/j.apsb.2025.02.019

Hao, Z., Ji, R., Su, Y., Wang, H., Yang, W., Zhang, S., Liu, Y., Ma, S., Guan, F., & Cui, Y. (2025). Indole-3-Propionic Acid Attenuates Neuroinflammation and Cognitive Deficits by Inhibiting the RAGE-JAK2-STAT3 Signaling Pathway. *Journal of Agricultural and Food Chemistry*, *73*(9), 5208–5222. Q1. https://doi.org/10.1021/acs.jafc.4c08548

He, X., Tian, Y., Lei, L., Zhi, Q., Zhao, J., & Ming, J. (2020). Protective effects of *Coreopsis tinctoria* buds extract against cognitive impairment and brain aging induced by d-galactose. *Journal of Functional Foods*, *73*, 104089. https://doi.org/10.1016/j.jff.2020.104089

Jiang, J., Wang, D., Jiang, Y., Yang, X., Sun, R., Chang, J., Zhu, W., Yao, P., Song, K., Chang, S., Wang, H., Zhou, L., Zhang, X.-S., Li, H., & Li, N. (2024). The gut metabolite indole-3-propionic acid. *Microbiome*, *12*(1), 66. Q1. https://doi.org/10.1186/s40168-024-01755-7

Jiang, Z.-M., Wang, F.-F., Zhao, Y.-Y., Lu, L.-F., Jiang, X.-Y., Huang, T.-Q., Lin, Y., Guo, L., Weng, Z.-B., & Liu, E.-H. (2024). *Hypericum perforatum* L. attenuates depression by regulating *Akkermansia muciniphila*, tryptophan metabolism and NFκB-NLRP2-Caspase1-IL1β pathway. *Phytomedicine: International Journal of Phytotherapy and Phytopharmacology*, *132*, 155847. https://doi.org/10.1016/j.phymed.2024.155847

Khan, A. S., & Langmann, T. (2020). Indole-3-carbinol regulates microglia homeostasis and protects the retina from degeneration. *Journal of Neuroinflammation*, *17*(1), 327. https://doi.org/10.1186/s12974-020-01999-8

Koekkoek, P. S., Kappelle, L. J., van den Berg, E., Rutten, G. E. H. M., & Biessels, G. J. (2015). Cognitive function in patients with diabetes mellitus: Guidance for daily car. *The Lancet Neurology*, *14*(3), 329–340. https://doi.org/10.1016/S1474-4422(14)70249-2

Lefèvre, A., Mavel, S., Nadal-Desbarats, L., Galineau, L., Attucci, S., Dufour, D., Sokol, H., & Emond, P. (2019). Validation of a global quantitative analysis methodology of tryptophan metabolites in mice using LC-MS. *Talanta*, *195*, 593–598. https://doi.org/10.1016/j.talanta.2018.11.094

Li, H., Xu, G., Wu, D., Li, J., Cui, J., & Liu, J. (2021). Effects of ethyl acetate extract from Coreopsis tinctoria on learning and memory impairment in D-galactose-induced aging mice and the underlying molecular mechanism. *Food & Function*, *12*(6), 2531–2542. Q2. https://doi.org/10.1039/D0FO03293J

Li, L., Yang, C., Jia, M., Wang, Y., Zhao, Y., Li, Q., Gong, J., He, Y., Xu, K., Liu, X., Chen, X., Hu, J., & Liu, Z. (2024). Synbiotic therapy with *Clostridium sporogenes* and xylan promotes gut-derived indole-3-propionic acid and improves cognitive impairments in an Alzheimer's disease mouse model. *Food & Function*, *15*(15), 7865–7882. https://doi.org/10.1039/D4FO00886C

Li, S., Cai, Y., Guan, T., Zhang, Y., Huang, K., Zhang, Z., Cao, W., & Guan, X. (2024). Quinic acid alleviates high-fat diet-induced neuroinflammation by inhibiting DR3/IKK/NF-κB signaling via gut microbial tryptophan metabolites. *Gut Microbes*, *16*(1), 2374608. https://doi.org/10.1080/19490976.2024.2374608

Li, Y., Chen, X., Xue, J., Liu, J., Chen, X., & Wulasihan, M. (2014). Flavonoids furom Coreopsis tinctoria adjust lipid metabolism in hyperlipidemia animals by down-regulating adipose differentiation-related protein. *Lipids in Health and Disease*, *13*(1), 193. Q2. https://doi.org/10.1186/1476-511X-13-193

Li, Y., Cui, Z., Li, Y., Gao, J., Tao, R., Li, J., Li, Y., & Luo, J. (2022). Integrated molecular networking strategy enhance the accuracy and visualization of components identification: A case study of *Ginkgo biloba* leaf extract. *Journal of Pharmaceutical and Biomedical Analysis*, *209*, 114523. https://doi.org/10.1016/j.jpba.2021.114523

Li, Y., Dang, Q., Shen, Y., Guo, L., Liu, C., Wu, D., Fang, L., Leng, Y., & Min, W. (2024). Therapeutic effects of a walnut-derived peptide on NLRP3 inflammasome activation, synaptic plasticity, and cognitive dysfunction in T2DM mice. *Food & Function*, *15*(4), 2295–2313. https://doi.org/10.1039/d3fo05076a

Liu, J., Pang, Y., Yang, H., Huo, D., Liu, X., & Chen, X. (2023). Gut microbiota and urine metabolomics based exploration of *Coreopsis tinctoria* Nutt. Tea on type 2 diabetic mellitus. *Arabian Journal of Chemistry*, *16*(9), 105037. https://doi.org/10.1016/j.arabjc.2023.105037

Liu, M., Yuan, J., Hu, W., Ke, C., Zhang, Y., Ye, Y., Zhong, D., Zhao, G., Yao, S., & Liu, J. (2019). Pretreatment with broad-spectrum antibiotics alters the pharmacokinetics of major constituents of Shaoyao-Gancao decoction in rats after oral administration. *Acta Pharmacologica Sinica*, *40*(2), 288–296. https://doi.org/10.1038/s41401-018-0011-0

Liu, Z., Dai, X., Zhang, H., Shi, R., Hui, Y., Jin, X., Zhang, W., Wang, L., Wang, Q., Wang, D., Wang, J., Tan, X., Ren, B., Liu, X., Zhao, T., Wang, J., Pan, J., Yuan, T., Chu, C., … Liu, X. (2020). Gut microbiota mediates intermittent-fasting alleviation of diabetes-induced cognitive impairment. *Nature Communications*, *11*(1), 855. https://doi.org/10.1038/s41467-020-14676-4

Luo, M., Han, Y., Chen, Y., Du, H., Chen, B., Gao, Z., Wang, Q., Cao, Y., & Xiao, H. (2024). Unveiling the role of gut microbiota in curcumin metabolism using antibiotic-treated mice. *Food Chemistry*, *460*, 140706. https://doi.org/10.1016/j.foodchem.2024.140706

Lv, Q., Wu, X., Guan, Y., Lin, J., Sun, Y., Hu, M., Xiao, P., He, C., & Jiang, B. (2023). Integration of network pharmacology, transcriptomics and molecular docking reveals two novel hypoglycemic components in snow chrysanthemum. *Biomedicine & Pharmacotherapy*, *163*, 114818. https://doi.org/10.1016/j.biopha.2023.114818

Nothias, L.-F., Petras, D., Schmid, R., Dührkop, K., Rainer, J., Sarvepalli, A., Protsyuk, I., Ernst, M., Tsugawa, H., Fleischauer, M., Aicheler, F., Aksenov, A. A., Alka, O., Allard, P.-M., Barsch, A., Cachet, X., Caraballo-Rodriguez, A. M., Da Silva, R. R., Dang, T., … Dorrestein, P. C. (2020). Feature-based molecular networking in the GNPS analysis environment. *Nature Methods*, *17*(9), 905–908. https://doi.org/10.1038/s41592-020-0933-6

Pan, W., Zhao, J., Wu, J., Xu, D., Meng, X., Jiang, P., Shi, H., Ge, X., Yang, X., Hu, M., Zhang, P., Tang, R., Nagaratnam, N., Zheng, K., Huang, X.-F., & Yu, Y. (2023). Dimethyl itaconate ameliorates cognitive impairment induced by a high-fat diet via the gut-brain axis in mice. *Microbiome*, *11*(1), 30. https://doi.org/10.1186/s40168-023-01471-8

Qian, X., Li, Q., Zhu, H., Chen, Y., Lin, G., Zhang, H., Chen, W., Wang, G., & Tian, P. (2024). Bifidobacteria with indole-3-lactic acid-producing capacity exhibit psychobiotic potential via reducing neuroinflammation. *Cell Reports Medicine*, *5*(11), 101798. https://doi.org/10.1016/j.xcrm.2024.101798

Ramos-García, N. A., Orozco-Ibarra, M., Estudillo, E., Elizondo, G., Gómez Apo, E., Chávez Macías, L. G., Sosa-Ortiz, A. L., & Torres-Ramos, M. A. (2020). Aryl Hydrocarbon Receptor in Post-Mortem Hippocampus and in Serum from Young, Elder, and Alzheimer's Patients. *International Journal of Molecular Sciences*, *21*(6), Article 6. https://doi.org/10.3390/ijms21061983

Shang, M., Ning, J., Zang, C., Ma, J., Yang, Y., Wan, Z., Zhao, J., Jiang, Y., Chen, Q., Dong, Y., Wang, J., Li, F., Bao, X., & Zhang, D. (2025). Microbial metabolite 3-indolepropionic acid alleviated PD pathologies by decreasing enteric glia cell gliosis *via* suppressing IL-13Rα1 related signaling pathways. *Acta Pharmaceutica Sinica B*, *15*(4), 2024–2038. https://doi.org/10.1016/j.apsb.2025.02.029

Shen, J., Hu, M., Tan, W., Ding, J., Jiang, B., Xu, L., Hamulati, H., He, C., Sun, Y., & Xiao, P. (2021). Traditional uses, phytochemistry, pharmacology, and toxicology of *Coreopsis tinctoria* Nutt.: A review. *Journal of Ethnopharmacology*, *269*, 113690. https://doi.org/10.1016/j.jep.2020.113690

Sun, J., Zhang, Y., Kong, Y., Ye, T., Yu, Q., Kumaran Satyanarayanan, S., Su, K.-P., & Liu, J. (2022). Microbiota-derived metabolite Indoles induced aryl hydrocarbon receptor activation and inhibited neuroinflammation in APP/PS1 mice. *Brain, Behavior, and Immunity*, *106*, 76–88. https://doi.org/10.1016/j.bbi.2022.08.003

Sun, P., Wang, M., Li, Z., Wei, J., Liu, F., Zheng, W., Zhu, X., Chai, X., & Zhao, S. (2022). *Eucommiae cortex* polysaccharides mitigate obesogenic diet-induced cognitive and social dysfunction via modulation of gut microbiota and tryptophan metabolism. *Theranostics*, *12*(8), 3637–3655. https://doi.org/10.7150/thno.72756

Wang, L.-S., Zhang, M.-D., Tao, X., Zhou, Y.-F., Liu, X.-M., Pan, R.-L., & Liao, Y.-H. (2019). LC-MS/MS-based quantification of tryptophan metabolites and neurotransmitters in the serum and brain of mice. *Journal of Chromatography B*, *1112*, 24–32. https://doi.org/10.1016/j.jchromb.2019.02.021

Wang, T., Chen, B., Luo, M., Xie, L., Lu, M., Lu, X., Zhang, S., Wei, L., Zhou, X., Yao, B., Wang, H., & Xu, D. (2023). Microbiota-indole 3-propionic acid-brain axis mediates abnormal synaptic pruning of hippocampal microglia and susceptibility to ASD in IUGR offspring. *Microbiome*, *11*(1), 245. https://doi.org/10.1186/s40168-023-01656-1

Wang, Y., Tong, Q., Shou, J.-W., Zhao, Z.-X., Li, X.-Y., Zhang, X.-F., Ma, S.-R., He, C.-Y., Lin, Y., Wen, B.-Y., Guo, F., Fu, J., & Jiang, J.-D. (2017). Gut Microbiota-Mediated Personalized Treatment of Hyperlipidemia Using Berberine. *Theranostics*, *7*(9), 2443–2451. https://doi.org/10.7150/thno.18290

Wei, G. Z., Martin, K. A., Xing, P. Y., Agrawal, R., Whiley, L., Wood, T. K., Hejndorf, S., Ng, Y. Z., Low, J. Z. Y., Rossant, J., Nechanitzky, R., Holmes, E., Nicholson, J. K., Tan, E.-K., Matthews, P. M., & Pettersson, S. (2021). Tryptophan-metabolizing gut microbes regulate adult neurogenesis via the aryl hydrocarbon receptor. *Proceedings of the National Academy of Sciences of the United States of America*, *118*(27), e2021091118. https://doi.org/10.1073/pnas.2021091118

Xue, C., Li, G., Zheng, Q., Gu, X., Shi, Q., Su, Y., Chu, Q., Yuan, X., Bao, Z., Lu, J., & Li, L. (2023). Tryptophan metabolism in health and disease. *Cell Metabolism*, *35*(8), 1304–1326. https://doi.org/10.1016/j.cmet.2023.06.004

Yin, J., Zhang, Y., Liu, X., Li, W., Hu, Y., Zhang, B., & Wang, S. (2023). Gut Microbiota-Derived Indole Derivatives Alleviate Neurodegeneration in Aging through Activating GPR30/AMPK/SIRT1 Pathway. *Molecular Nutrition & Food Research*, *67*(9), 2200739. https://doi.org/10.1002/mnfr.202200739

Zhang, J., Chen, C., Hua, S., Liao, H., Wang, M., Xiong, Y., & Cao, F. (2017). An updated meta-analysis of cohort studies: Diabetes and risk of Alzheimer's disease. *Diabetes Research and Clinical Practice*, *124*, 41–47. https://doi.org/10.1016/j.diabres.2016.10.024

Zhang, S., Wang, X., Liu, S., Hu, C., & Meng, Y. (2025). Phlorizin ameliorates cognitive and behavioral impairments via the microbiota-gut-brain axis in high-fat and high-fructose diet-induced obese male mice. *Brain, Behavior, and Immunity*, *123*, 193–210. Q1. https://doi.org/10.1016/j.bbi.2024.09.008

Zhou, M., Fan, Y., Xu, L., Yu, Z., Wang, S., Xu, H., Zhang, J., Zhang, L., Liu, W., Wu, L., Yu, J., Yao, H., Wang, J., & Gao, R. (2023). Microbiome and tryptophan metabolomics analysis in adolescent depression: Roles of the gut microbiota in the regulation of tryptophan-derived neurotransmitters and behaviors in human and mice. *Microbiome*, *11*(1), 145. https://doi.org/10.1186/s40168-023-01589-9